



저작자표시-비영리-변경금지 2.0 대한민국

이용자는 아래의 조건을 따르는 경우에 한하여 자유롭게

- 이 저작물을 복제, 배포, 전송, 전시, 공연 및 방송할 수 있습니다.

다음과 같은 조건을 따라야 합니다:



저작자표시. 귀하는 원저작자를 표시하여야 합니다.



비영리. 귀하는 이 저작물을 영리 목적으로 이용할 수 없습니다.



변경금지. 귀하는 이 저작물을 개작, 변형 또는 가공할 수 없습니다.

- 귀하는, 이 저작물의 재이용이나 배포의 경우, 이 저작물에 적용된 이용허락조건을 명확하게 나타내어야 합니다.
- 저작권자로부터 별도의 허가를 받으면 이러한 조건들은 적용되지 않습니다.

저작권법에 따른 이용자의 권리는 위의 내용에 의하여 영향을 받지 않습니다.

이것은 [이용허락규약\(Legal Code\)](#)을 이해하기 쉽게 요약한 것입니다.

[Disclaimer](#)

Master's Thesis

Ultraconcentrated Sodium Bis(fluorosulfonyl)imide-
Based Electrolytes for High-Performance Sodium
Metal Batteries

Jaegi Lee

Department of Energy Engineering
(Battery Science and Technology)

Graduate School of UNIST

2017

Ultraconcentrated Sodium
Bis(fluorosulfonyl)imide-Based Electrolytes for
High-Performance Sodium Metal Batteries

Jaegi Lee

Department of Energy Engineering
(Battery Science and Technology)

Graduate School of UNIST

Ultraconcentrated Sodium
Bis(fluorosulfonyl)imide-Based Electrolytes for
High-Performance Sodium Metal Batteries

A thesis
submitted to the Graduate School of UNIST
in partial fulfillment of the
requirements for the degree of
Master of Science

Jaegi Lee

06. 05. 2017 of submission

Approved by

Nam-Soon Choi

Advisor

Nam-Soon Choi

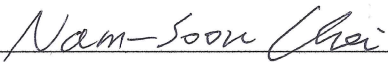
Ultraconcentrated Sodium
Bis(fluorosulfonyl)imide-Based Electrolytes for
High-Performance Sodium Metal Batteries

Jaegi Lee

This certifies that the thesis/dissertation of Jaegi Lee is approved.

06/05/2017

signature



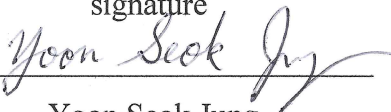
Advisor: Nam-Soon Choi

signature



Soojin Park

signature



Yoon Seok Jung

Abstract

Rechargeable Na metal batteries have gained great recognition as a promising candidate for next-generation battery systems, largely on the basis of the high theoretical specific capacity (1165 mAh g⁻¹) and low redox potential (-2.71 V versus the standard hydrogen electrode) of Na metal, as well as the natural abundance of Na and the similarities between these batteries and lithium batteries. Much effort has been dedicated to improving the electrochemical performance of rechargeable Na batteries through the development of high-performance cathodes, anodes, and electrolytes. Nevertheless, the practical application of Na metal batteries is quite challenging because the high chemical and electrochemical reactivity of Na metal electrodes with organic liquid electrolytes leads to low Coulombic efficiencies and limited cycling performance. Severe electrolyte decomposition at the Na metal electrode results in the formation of a resistive and non-uniform surface film, leading to dendritic Na metal growth. To control the Na metal electrode–electrolyte interface for high performance Na metal batteries, considerable efforts have been made to find electrolyte systems that are stable at the Na metal electrode. Using fluoroethylene carbonate (FEC) as an electrolyte additive for in situ formation of an artificial solid electrolyte interphase (SEI) layer could stabilize the anode–electrolyte interface. However, the FEC-derived SEI acted as a resistive layer, impeding the sodiation–desodiation process and reducing the reversible capacity of the anodes. Finding new electrolyte systems that are stable at the Na metal electrode and possess high oxidation durability at high-voltage cathodes is necessary for the development of high-performance Na metal batteries.

Very recently, there are some papers which introduced significant breakthroughs in lithium battery electrolytes. It is reported that improving the cycling efficiency of lithium plating/stripping and suppressing the formation of dendritic lithium metal is possible by using highly concentrated electrolytes, even at high current densities. And it is also reported that highly concentrated electrolytes can inhibit the dissolution of transition metals out of the 5 V-class LiNi_{0.5}Mn_{1.5}O₄ (LNMO) electrode material and the corrosion of the Al current collector at high voltage conditions. After reading these papers, I thought that applying this highly concentrated electrolyte system to sodium metal batteries could be the solution for improvements in the electrochemical performance of Na metal anodes coupled with high-voltage cathodes.

In this study, an ultraconcentrated electrolyte composed of 5 M sodium bis(fluorosulfonyl)imide in 1,2-dimethoxyethane will be introduced for Na metal anodes coupled with high-voltage cathodes. Using this electrolyte, a very high Coulombic efficiency of 99.3% at the 120th cycle for Na plating/stripping is obtained in Na/stainless steel (SS) cells, with highly reduced corrosivity toward Na metal and high oxidation durability (over 4.9 V versus Na/Na⁺) without corrosion of the aluminum cathode current collector. Importantly, the use of this ultraconcentrated electrolyte results in substantially improved rate capability in Na/SS cells and excellent cycling performance in Na/Na

symmetric cells without the increase of polarization. Moreover, this ultraconcentrated electrolyte exhibits good compatibility with high-voltage $\text{Na}_4\text{Fe}_3(\text{PO}_4)_2(\text{P}_2\text{O}_7)$ and $\text{Na}_{0.7}(\text{Fe}_{0.5}\text{Mn}_{0.5})\text{O}_2$ cathodes charged to high voltages (>4.2 V versus Na/Na^+), resulting in outstanding cycling stability (high reversible capacity of 109 mAh g^{-1} over 300 cycles for the $\text{Na}/\text{Na}_4\text{Fe}_3(\text{PO}_4)_2(\text{P}_2\text{O}_7)$ cell) compared with the conventional dilute electrolyte, 1 M NaPF_6 in ethylene carbonate/propylene carbonate (5/5, v/v).

Contents

I. Introduction

1.1 Demand for Na metal batteries-----	9
1.2 Problems of Na metal batteries-----	11
1.3 New electrolyte systems : highly concentrated electrolytes-----	13

II. Experimental

2.1 Electrolytes and electrodes -----	16
2.2 Characterization -----	17
2.3 Electrochemical tests -----	18

III. Result and Discussion

3.1 Properties of ultraconcentrated electrolytes-----	19
3.2 Three mechanisms of improved oxidation durability of 5M NaFSI-DME-----	24
3.3 Electrochemical performances of Na/SS cells and analysis-----	27
3.4 Electrochemical performances of Na/Na symmetric cells and analysis-----	31
3.5 Electrochemical performances of Na/Cathode cells and analysis-----	33

IV. Conclusion-----	38
---------------------	----

V. References -----	39
---------------------	----

List of figures

Figure 1. An schematic representation of Na battery.

Figure 2. ^{13}C NMR spectra of (a) DMC-added electrolyte and (b) DMC + FEC-added electrolyte before and after contact with Na metal for 10 days without applied potentials. Schematic representation of (c) the formation of decomposed products by the reaction between DMC and Na metal and (d) the suppression of the decomposition of DMC by addition of 5 wt% FEC, which can make a protective surface film on Na metal.

Figure 3. SEM images of the morphologies of Li metal after plating on Cu substrates in different electrolytes. (a,b) 1M LiPF₆-PC. (c,d) 4M LiFSI-DME. The current density was 1.0mAcm⁻² and the deposition time was 1.5 h. The diameter of the Cu substrate shown in the insert of (a,c) was 2 cm. Scale bar, 10 μm .

Figure 4. Oxidation stability of an aluminium electrode. LSV of an aluminium electrode in various concentrations of LiFSA/DMC electrolytes in a three-electrode cell. The scan rate was 1.0mVs⁻¹. The insets are scanning electron microscopy images of the Al surface polarized in the dilute 1:10.8 (left of panel) and superconcentrated 1:1.1 (right of panel) electrolytes. Many corroding pits cover the surface of the Al electrode polarized in the dilute electrolyte, showing a severe anodic Al dissolution. In contrast, no corroding pits appear on the surface of the Al electrode polarized in the superconcentrated electrolyte, indicating a good inhibition of anodic Al dissolution. The white scale bar represents 20 μm .

Figure 5. (a) Photograph of 1 and 5 M NaFSI-DME in Eppendorf tubes. (b) Ionic conductivity of x M NaFSI-DME, x M NaPF₆-EC/PC (5/5), x M NaFSI-EC/PC, and 1 M NaPF₆-DME, and viscosity of x M NaFSI-DME at room temperature. (c) FTIR spectra of x M NaFSI-DME ($x = 0, 1, 2, 3, 4,$ and 5) and pure NaFSI salt. (d) Anodic limits of conventional dilute and highly concentrated electrolytes on an Al working electrode at a scan rate of 1 mV s⁻¹.

Figure 6. Photograph showing the solubility limit of NaFSI in DME solvent.

Figure 7. Relative fraction of solvated and free DME, and FSI⁻ anion participating in the solvation of Na⁺ cation as a function of the NaFSI salt concentration (Top). FT-IR peak fitting was performed to calculate the relative fraction of three peaks (Bottom).

Figure 8. SEM images of (a) pristine Al and Al surfaces after LSV measurements in (b) 1 M NaFSI-DME and (c) 5 M NaFSI-DME (NaFSI : DME = 1.06 : 1 mole ratio) (scale bar: 100 μm).

Figure 9. F 1s and Al 2p XPS spectra of Al electrodes after the LSV measurements.

Figure 10. Photograph of Na metal electrodes after contact with 1M NaFSI-DME or 5M NaFSI-DME for 5 days.

Figure 11. Anodic limits of 1M NaFSI-DME and 5M NaFSI-DME on a Pt electrode at a scan rate of

1 mV s⁻¹. The inset displays the enlarged LSV data for the comparison of anodic limits of 5M NaFSI-DME on Al and Pt electrode. The disc-type Pt electrode (area=1.77cm²) was used as a working electrode.

Figure 12. (a) Voltage profiles for initial Na plating/stripping in the coin-type Na/SS cells at a rate of C/10 (0.056 mA cm⁻²). (b) Voltage profiles of 5 M NaFSI-DME during the 1st, 5th, 10th, 50th, and 100th cycles at a rate of C/10. (c) Coulombic efficiency for Na plating/stripping in Na/SS cells. (d) Coulombic efficiency of Na/SS cells with 5 M NaFSI-DME and 1 M NaPF₆ EC/PC (5/5) at various C rates. (e) Photographs of a pristine Na metal electrode and Cu substrates after the initial Na plating at a rate of C/10. The utilized capacity of the Na metal electrode was 5.0 mAh.

Figure 13. Coulombic efficiency of Na/SS cells during 100 cycles at a 1 C rate (corresponding to a current density of 0.56 mA cm⁻²) after precycling at a C/10 rate. 5 M NaFSI-DME with and without 1 wt% FEC was used as the electrolyte. The utilized capacity of the Na metal electrode was 1.0 mAh.

Figure 14. A comparison of SEM images and EDS patterns of Na deposit on Cu substrates with 1 M NaPF₆-EC/PC (5/5) and 5 M NaFSI-DME after the initial Na plating at a rate of C/10. The utilized capacity of the Na metal electrode was 5.0 mAh.

Figure 15. (a) Galvanostatic cycling of Na/Na symmetric cells during 600 cycles with the time cut-off condition of 0.5 h at a current density of 0.0028 mA cm⁻² after precycling at a current density of 0.0014 mA cm⁻². (b) Enlarged region showing the voltage profiles for the 561st to 570th cycles.

Figure 16. (a) Initial voltage profiles of Na/Na₄Fe₃(PO₄)₂(P₂O₇) full cells at a rate of C/20. (b) Discharge capacity and (c) Coulombic efficiency of Na/Na₄Fe₃(PO₄)₂(P₂O₇) full cells during 300 cycles at a rate of C/2. (d) Initial voltage profiles of Na/Na_{0.7}(Fe_{0.5}Mn_{0.5})O₂ full cells at a rate of C/20. (e) Discharge capacity and (f) Coulombic efficiency of Na/Na_{0.7}(Fe_{0.5}Mn_{0.5})O₂ full cells during 100 cycles at a rate of C/2.

Figure 17. Voltage–capacity profiles of the Na₄Fe₃(PO₄)₂(P₂O₇) cathode during the 5th, 10th, 20th, 50th, and 100th cycles in (a) 1 M NaPF₆-EC/PC (5/5) and (b) 5 M NaFSI-DME at a rate of C/2. Voltage–capacity profiles of the Na_{0.7}(Fe_{0.5}Mn_{0.5})O₂ cathode in (c) 1 M NaPF₆-EC/PC (5/5) and (d) 5 M NaFSI-DME at a rate of C/2.

Figure 18. Voltage profiles of the Na₄Fe₃(PO₄)₂(P₂O₇) cathode during precycling at a rate of C/20. The inset photographs show Na metal electrodes and GFF separators retrieved from Na/Na₄Fe₃(PO₄)₂(P₂O₇) cells with 1 M, 4 M, or 5 M NaFSI-DME after precycling. For comparison, the voltage profiles of the Na₄Fe₃(PO₄)₂(P₂O₇) cathode with 1 M NaPF₆-EC/PC (5/5) and photographs of the retrieved Na metal electrodes and GFF separators are included.

Figure 19. XRD pattern of the synthesized Na_{0.7}(Fe_{0.5}Mn_{0.5})O₂ cathode.

I. Introduction

1.1 Demand for Na metal batteries

Rechargeable Na metal batteries have gained great recognition as a promising candidate for next-generation battery systems, largely on the basis of the high theoretical specific capacity (1165 mAh g⁻¹) and low redox potential (-2.71 V versus the standard hydrogen electrode) of Na metal, as well as the natural abundance of Na and the similarities between these batteries and lithium batteries.¹⁻³ Also, there is another factor which makes Na batteries more cost effective than Li batteries. For Li batteries, since aluminum (Al) can form a binary alloy with Li, copper (Cu) is used as a current collector for negative electrode materials. In contrast, Na does not form an alloy with Al that can be used as the current collector for Na batteries. Using more cheaper Al as a current collector for negative electrode is an additional practical advantage of the Na batteries system, which could reduce the total cost of batteries, compared to Li batteries.¹ There is a schematic representation of Na battery in Figure 1.

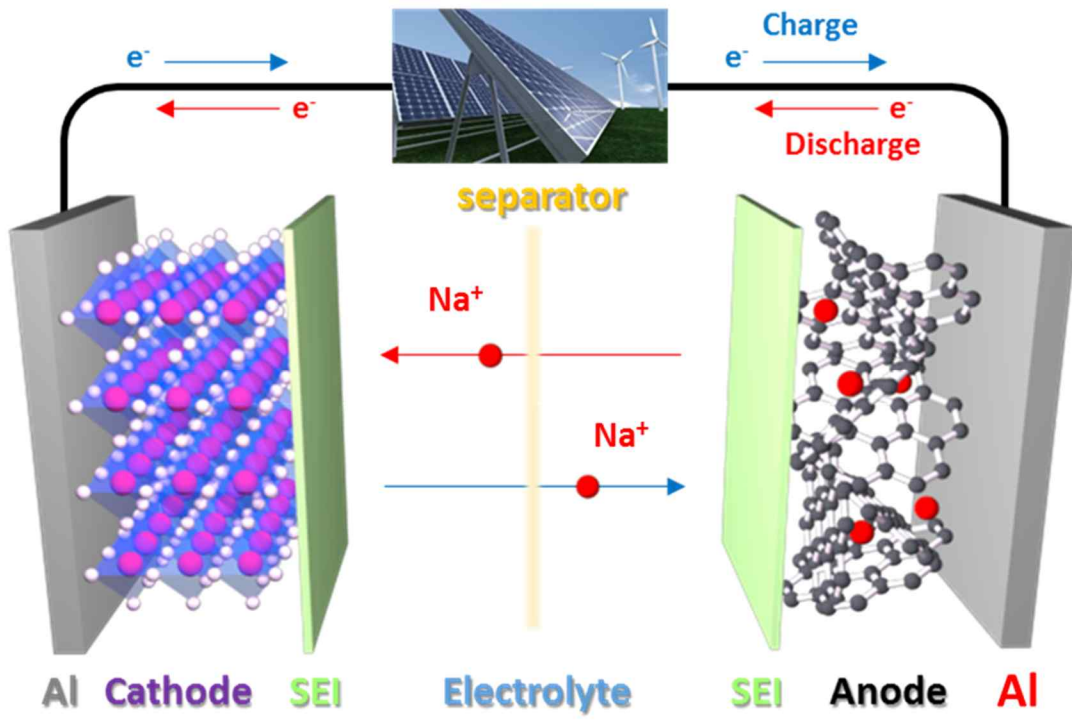


Figure 1. An schematic representation of Na battery.

1.2 Problems of Na metal batteries

Much effort has been dedicated to improving the electrochemical performance of rechargeable Na batteries through the development of high-performance cathodes,⁴⁻¹⁴ anodes,¹⁵⁻¹⁹ and electrolytes.²⁰⁻²⁷ Nevertheless, the practical application of Na metal batteries is quite challenging because the high chemical and electrochemical reactivity of Na metal electrodes with organic liquid electrolytes leads to low Coulombic efficiencies and limited cycling performance.^{20,24-26} Severe electrolyte decomposition at the Na metal electrode results in the formation of a resistive and non-uniform surface film, leading to dendritic Na metal growth. To control the Na metal electrode–electrolyte interface for high performance Na metal batteries, considerable efforts have been made to find electrolyte systems that are stable at the Na metal electrode.^{20,21,23-26} The use of linear carbonates such as dimethyl carbonate (DMC), which are widely used as electrolyte solvents in lithium batteries, is limited due to their drastic decomposition at Na metal electrodes and sodiated hard carbon anodes.^{24,27} Using fluoroethylene carbonate (FEC) as an electrolyte additive for *in situ* formation of an artificial solid electrolyte interphase (SEI) layer could stabilize the anode–electrolyte interface (Figure 2).^{22,24,26} However, the FEC-derived SEI acted as a resistive layer, impeding the sodiation–desodiation process and reducing the reversible capacity of the anodes.²² Finding new electrolyte systems that are stable at the Na metal electrode and possess high oxidation durability at high-voltage cathodes is necessary for the development of high-performance Na metal batteries.

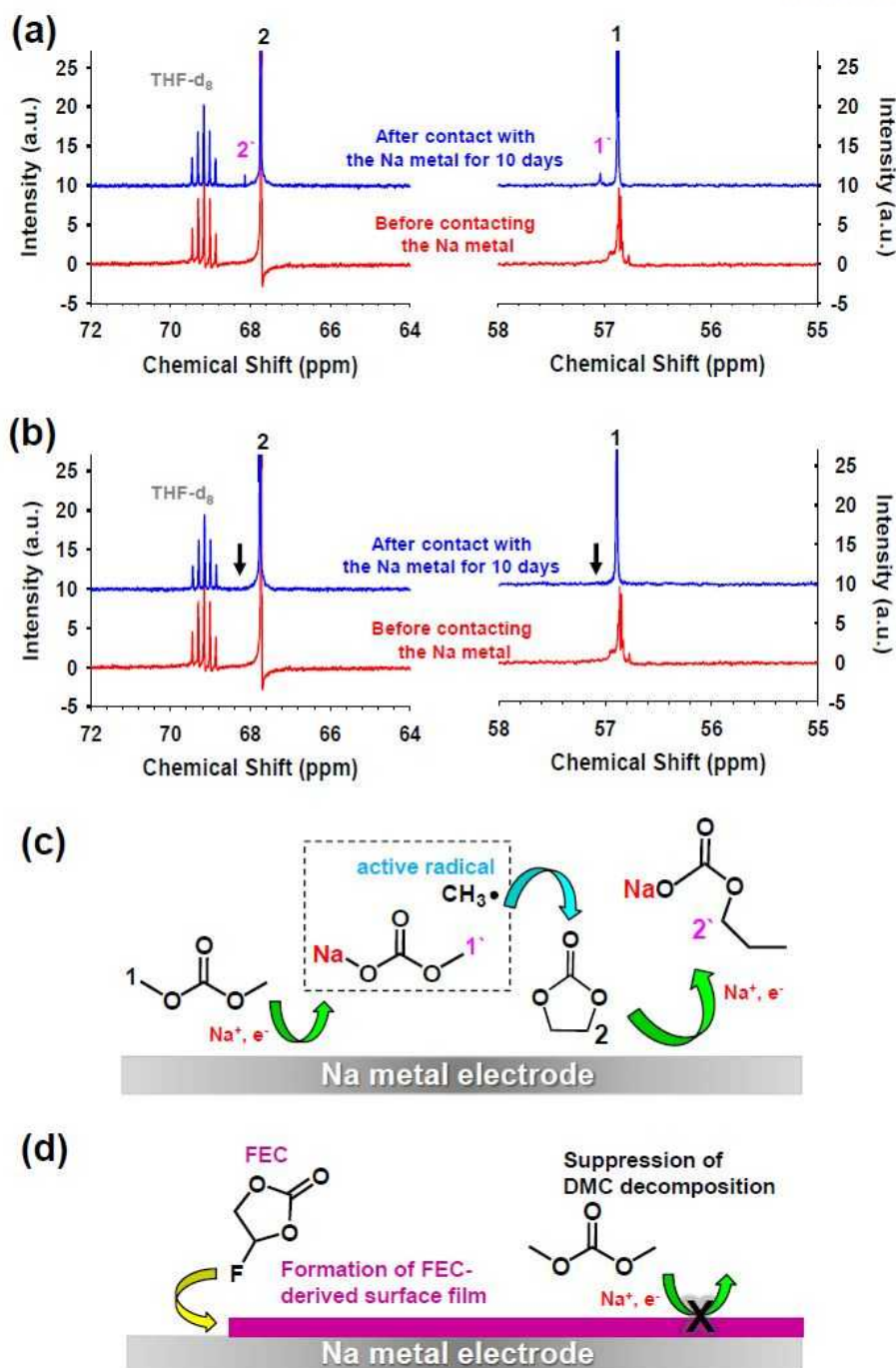


Figure 2. ^{13}C NMR spectra of (a) DMC-added electrolyte and (b) DMC + FEC-added electrolyte before and after contact with Na metal for 10 days without applied potentials. Schematic representation of (c) the formation of decomposed products by the reaction between DMC and Na metal and (d) the suppression of the decomposition of DMC by addition of 5 wt% FEC, which can make a protective surface film on Na metal.¹⁴

1.3 New electrolyte systems : highly concentrated electrolytes

Recently, the Zhang and Yamada groups reported significant breakthroughs in lithium battery electrolytes.^{28,29} A highly concentrated electrolyte, 4 M lithium bis(fluorosulfonyl)imide (LiN(SO₂F)₂, LiFSI) in 1,2-dimethoxyethane (DME or glyme), drastically improved the cycling efficiency of lithium plating/stripping and suppressed the formation of dendritic lithium metal, even at high current densities (Figure 3).²⁸ A superconcentrated electrolyte based on lithium bis(fluorosulfonyl)amide (LiFSA or LiFSI)-DMC (1:1.1 molar ratio) effectually inhibited the dissolution of transition metals out of the 5 V-class LiNi_{0.5}Mn_{1.5}O₄ (LNMO) electrode material and the corrosion of the Al current collector at high voltage conditions (Figure 4).²⁹ Moreover, the cycling stability, high rate capability, and safety of a high-voltage LiNi_{0.5}Mn_{1.5}O₄/graphite battery were greatly improved by the use of the superconcentrated LiFSA-DMC electrolyte.²⁹ Since highly concentrated liquid electrolyte systems were first suggested by the McKinnon and Dahn groups, many research groups have concentrated on the distinctive functions of such systems.²⁸⁻⁴⁰ Unwanted co-intercalation of propylene carbonate (PC) into a layered ZrS₂ electrode could be mitigated by using a saturated solution of LiAsF₆ in PC.³⁰ Highly concentrated PC electrolytes with 2.72 M LiN(SO₂C₂F₅)₂ allowed the use of graphite as an anode in lithium-ion batteries, which is exfoliated in PC electrolytes with low salt concentrations of around 0.82 M.³¹ Moreover, good cycling efficiency for lithium plating/stripping and suppression of dendritic lithium growth have been achieved in highly concentrated PC-based electrolytes.³² The Yamada group reported that the use of 4.2 M lithium bis(trifluoromethanesulfonyl)amide (LiTFSA or LiTFSI) in acetonitrile (AN) drastically enhanced reductive stability at low potentials for lithium intercalation into a graphite electrode and that the use of 4.5 M LiFSA in AN allowed not only good reductive stability but also relatively fast electrochemical reaction kinetics of a graphite electrode when compared with commercially used electrolyte systems.³⁴ Additionally, Al corrosion was not observed up to 4.5 V versus Li/Li⁺ and good cycling performance of a 4 V-class Li/LiMn₂O₄ cell at high rates was achieved in a highly concentrated LiFSA-AN-based electrolyte.³⁷ Very recently, the Zhang group reported that a highly concentrated electrolyte based on sodium bis(fluorosulfonyl)imide (NaFSI) enables the use of Na metal anodes for room-temperature sodium metal batteries based on a Na₃V₂(PO₄)₃ cathode with the charging cut-off voltage of 3.7 V versus Na/Na⁺.⁴¹ The Freunberger group demonstrated that a highly concentrated NaFSI-DME electrolyte allows nondendritic Na metal plating and its good compatibility with Na intercalation electrodes (Na₃V₂(PO₄)₃ cathodes and hard carbon anodes) makes reliable evaluation of half cells possible.⁴² Additionally, it was reported that highly concentrated NaTFSI-dimethyl sulfoxide (DMSO) electrolyte improves the cycling performance of Na-O₂ batteries.⁴³ Herein, we demonstrate that the use of an ultraconcentrated electrolyte composed of 5 M NaFSI in DME leads to high Coulombic efficiency for Na

plating/stripping in Na/stainless steel (SS) cells and excellent oxidation stability of over 4.9 V versus Na/Na⁺ on the Al substrate used as the cathode current collector, which is impossible in dilute DME-based electrolytes. Moreover, we report for the first time that Na metal anodes coupled with high-voltage cathodes with high charging cut-off voltage of 4.3 V versus Na/Na⁺, Na₄Fe₃(PO₄)₂(P₂O₇) and Na_{0.7}(Fe_{0.5}Mn_{0.5})O₂, display superior electrochemical performance with this ultraconcentrated electrolyte than with the conventional dilute electrolyte of 1 M NaPF₆-ethylene carbonate (EC)/PC (5/5, v/v).

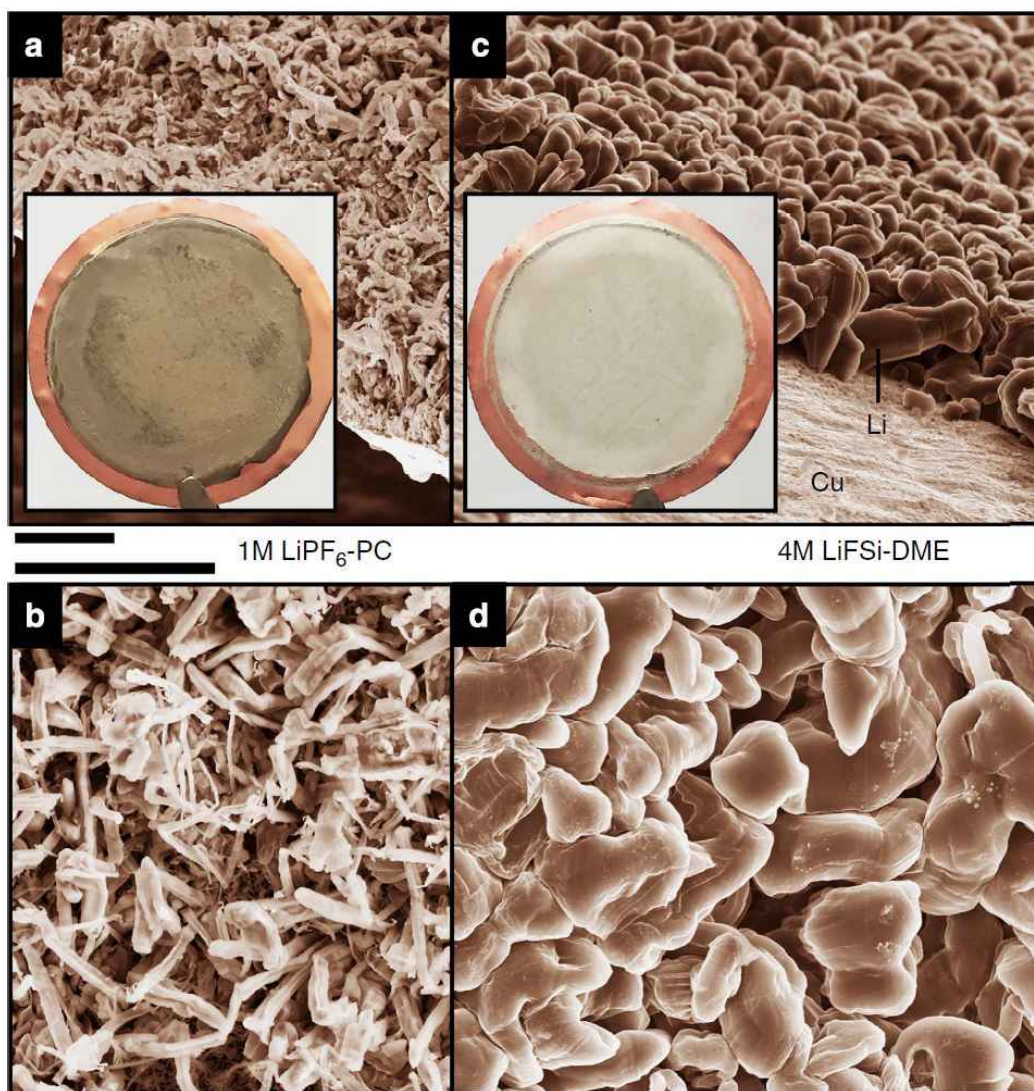


Figure 3. SEM images of the morphologies of Li metal after plating on Cu substrates in different electrolytes. (a,b) 1M LiPF₆-PC. (c,d) 4M LiFSI-DME. The current density was 1.0mAcm⁻² and the deposition time was 1.5 h. The diameter of the Cu substrate shown in the insert of (a,c) was 2 cm. Scale bar, 10 μm.²⁸

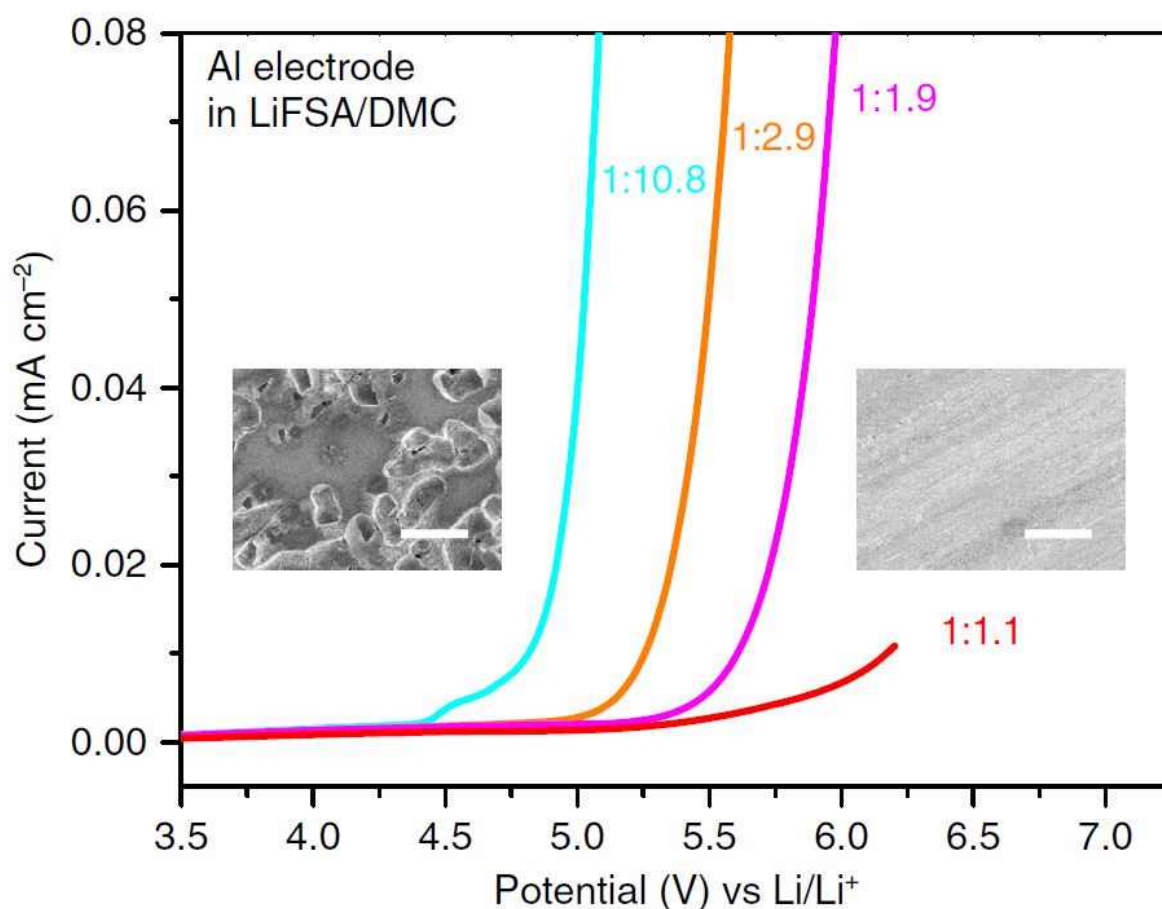


Figure 4. Oxidation stability of an aluminium electrode. LSV of an aluminium electrode in various concentrations of LiFSA/DMC electrolytes in a three-electrode cell. The scan rate was 1.0mVs^{-1} . The insets are scanning electron microscopy images of the Al surface polarized in the dilute 1:10.8 (left of panel) and superconcentrated 1:1.1 (right of panel) electrolytes. Many corroding pits cover the surface of the Al electrode polarized in the dilute electrolyte, showing a severe anodic Al dissolution. In contrast, no corroding pits appear on the surface of the Al electrode polarized in the superconcentrated electrolyte, indicating a good inhibition of anodic Al dissolution. The white scale bar represents $20\ \mu\text{m}$.²⁹

II. Experimental

2.1 Electrolytes and electrodes

The electrolytes were prepared by dissolving the salt (sodium bis(fluorosulfonyl)imide (NaFSI, $\geq 99.7\%$, Solvionic) or sodium hexafluorophosphate (NaPF₆, $\geq 99.0\%$, Alfa Aesar)) in the solvent (1,2-dimethoxyethane (DME, $\geq 99.9\%$, Aldrich) or a mixture of ethylene carbonate (EC)/propylene carbonate (PC) (5/5, v/v) (Soulbrain Co., Ltd.)). The Na₄Fe₃(PO₄)₂(P₂O₇) cathode material was synthesized according to a literature procedure.⁶ For the electrochemical tests, the electrode was prepared by spreading a slurry mixture of 70 wt% Na₄Fe₃(PO₄)₂(P₂O₇) as an active material, 20 wt% super P as a conducting agent, and 10 wt% poly(vinylidene fluoride) (PVDF) as a binder dissolved in anhydrous *N*-methyl-2-pyrrolidone (NMP, 99.5%, Aldrich) onto an Al foil.

The Na_{0.7}(Fe_{0.5}Mn_{0.5})O₂ cathode material was synthesized using a one-step solid-state method. The starting materials, Fe₃O₄ (98%, Aldrich), Mn₂O₃ (99%, Aldrich), and Na₂CO₃ (99.8%, Aldrich), were mixed with acetone using a planetary ball mill for 1 h at 300 rpm, and the mixed materials were then dried to remove acetone at 25 °C. The resulting mixture was sintered at 900 °C for 10 h in air to obtain the P2-type Na_{0.7}(Fe_{0.5}Mn_{0.5})O₂ cathode material. It was reported that cathodes with P2-type structures of Na_x(Fe_{0.5}Mn_{0.5})O₂ ($x \leq 0.71$) show relatively good cycling performance when compared with O₃ structures.^{44,45} X-ray diffraction (XRD) data for the Na_{0.7}(Fe_{0.5}Mn_{0.5})O₂ cathode were obtained using a Bruker D2 Phaser powder diffractometer equipped with a Cu-K α radiation source ($\lambda = 1.54184$ Å). The samples were scanned over the 2θ range of 15–80°. The structure of Na_{0.7}(Fe_{0.5}Mn_{0.5})O₂ corresponds to a hexagonal structure (Powder Diffraction File# 52-0537). For the electrochemical tests, the electrode was prepared by spreading a slurry mixture of 80 wt% Na_{0.7}(Fe_{0.5}Mn_{0.5})O₂ as an active material, 10 wt% super P as a conducting agent, and 10 wt% PVDF as a binder dissolved in anhydrous NMP (99.5%, Aldrich) onto an Al foil. The slurry was dried in a convection oven at 110 °C for 1 h. After drying, the electrodes were pressed and then dried under vacuum at 120 °C for 2 h prior to their assembly into cells. The thickness, specific capacity, and loading density of the Na₄Fe₃(PO₄)₂(P₂O₇) cathode were 45 μm , 0.254 mAh cm⁻², and 2 mg cm⁻², respectively. The thickness, specific capacity, and loading density of the Na_{0.7}(Fe_{0.5}Mn_{0.5})O₂ cathode were 34 μm , 0.7 mAh cm⁻², and 3.6 mg cm⁻², respectively.

2.2 Characterization

The ionic conductivity and viscosity of the electrolytes at room temperature were measured using an Oakton CON 11 standard conductivity meter and a Brookfield viscometer (LVDV-II+P), respectively. The attenuated total reflectance-Fourier transform infrared (ATR-FTIR) spectra of the electrolytes were recorded by reflectance measurements obtained using a Varian 670-IR spectrometer with a spectral resolution of 4 cm^{-1} under a nitrogen atmosphere. Scanning electron microscope (SEM; JSM-6700F, JEOL) images of Al working electrodes after linear sweep voltammetry (LSV) measurements and the Na metal plated on the Cu substrate were recorded using an FEI Nanonova 230. During the acquisition of the SEM image of the Na metal plated on the Cu substrate, an energy dispersive spectrometer (EDS) was used to determine the kind of chemical components. Each electrode was rinsed with DME to remove the residual electrolyte and then was dried at room temperature.

2.3 Electrochemical tests

The anodic limits of the electrolytes were determined by LSV using an Iviumstat (Ivium Technologies) at a scan rate of 1 mV s^{-1} . Al was used as the working electrode, with Na metal as the counter and reference electrodes. To evaluate the cycling efficiency and rate capability for the Na metal plating/stripping process, a 2032 coin-type cell with an SS electrode, a Na metal electrode, and a glass fiber filter (GFF, Whatman, $260 \mu\text{m}$ thickness) separator was assembled in an argon filled glove box with less than 1 ppm of both oxygen and moisture. Precycling and subsequent cycling of the Na/SS cells were galvanostatically performed at a current density of 0.056 mA cm^{-2} (corresponding to a C/10 rate) using a computer-controlled battery measurement system (WonATech WBCS 3000) at $30 \text{ }^\circ\text{C}$. During the first cathodic scan, Na plating occurred on the SS electrode, while Na was stripped from the Na counter electrode until the potential reached 1.0 V versus Na/Na⁺. The evaluation of the rate capability of the Na/SS cells was carried out at various current densities of 0.056 mA cm^{-2} (C/10), 0.19 mA cm^{-2} (C/3), 0.28 mA cm^{-2} (C/2), 0.56 mA cm^{-2} (1 C), 1.12 mA cm^{-2} (2 C), and 2.80 mA cm^{-2} (5 C) at $30 \text{ }^\circ\text{C}$.

To obtain the images of Na metal plated on a Cu substrate, a 2032 coin-type cell with a Cu electrode, a Na metal electrode, and a microporous polyethylene (PE) separator (thickness: $20 \mu\text{m}$, porosity: 38%, SK Innovation Co., Ltd.) was cycled at a rate of C/10 and the capacity of Na metal plated on the Cu substrate was 5 mAh. For electrochemical tests of Na/Na symmetrical cells, a 2032 coin-type cell with a Na working electrode and a Na metal electrode used as a counter electrode was assembled in an argon filled glove box with less than 1 ppm of both oxygen and moisture. After precycling at a current density of $0.0014 \text{ mA cm}^{-2}$, the Na stripping and deposition process was performed for 0.5 h at a current density of $0.0028 \text{ mA cm}^{-2}$. A 2032 coin-type full cell with a Na₄Fe₃(PO₄)₂(P₂O₇) or Na_{0.7}(Fe_{0.5}Mn_{0.5})O₂ cathode, a Na metal electrode, and a GFF separator was assembled in an argon filled glove box with less than 1 ppm of both oxygen and moisture. The Na/Na₄Fe₃(PO₄)₂(P₂O₇) cells were precycled in the potential window between 1.7 V and 4.2 V at a rate of C/20 at $30 \text{ }^\circ\text{C}$. Precycling of the Na/Na_{0.7}(Fe_{0.5}Mn_{0.5})O₂ cells was performed in the potential window between 1.5 V and 4.3 V at a rate of C/20 at $30 \text{ }^\circ\text{C}$. After precycling, the Na/cathode cells were cycled at a rate of C/2 at $30 \text{ }^\circ\text{C}$.

III. Result and discussion

3.1 Properties of ultraconcentrated electrolytes

The highly concentrated electrolyte composed of 5 M NaFSI dissolved in DME was transparent and viscous at room temperature (Figure 5a). This viscous electrolyte flowed through an Eppendorf tube, unlike the low concentration electrolyte 1 M NaFSI-DME. Changes in the structure of a solvent owing to ion–dipole interactions between the solvent molecule and an ionic species lead to an appreciable increase in the viscosity of the electrolyte.^{28,29} The viscosity of the NaFSI-DME electrolyte dramatically increased from 0.92 cP to 330.4 cP as the NaFSI salt concentration increased from 1 M to 5 M, and thus, the ionic conductivity of the concentrated electrolyte was significantly reduced (Figure 5b). The solubility limit of NaFSI in DME was 5 M (Figure 6). Concentrations of NaPF₆ greater than 2 M could not be dissolved in the mixed solvent EC/PC (5/5, v/v), and the ionic conductivity of the NaPF₆-EC/PC electrolyte was lower than that of NaFSI-DME at the same salt concentration. xM NaFSI-EC/PC electrolytes showed slightly reduced ionic conductivity compared with xM NaFSI-DME (Figure 5b). This is mostly due to high viscosity of EC/PC hampering the charge transport and causing a decrease in ionic conductivity. NaFSI-DME exhibited the highest ionic conductivity in the order of NaFSI-DME > NaPF₆-DME > NaFSI-EC/PC > NaPF₆-EC/PC at the salt concentration of 1 M in DME or a mixture of EC/PC (5/5). It is found that DME with low viscosity (0.455cP) is more effective solvent for fast movement of charge carriers compared with EC (1.9cP @40°C)/PC (2.53cP). 1 M NaFSI-DME showed slightly higher ionic conductivity (15.1 mS cm⁻¹) than 1 M NaPF₆-DME (11.1 mS cm⁻¹), presumably because of the increase of the number of charge carriers by higher NaFSI salt dissociation in DME. It is noteworthy that LiFSI with weakly coordinating FSI⁻ anions by delocalization of the negative charge over the whole anion is more readily dissociated in organic solvents than LiPF₆.⁴⁶ The Fourier transform infrared (FTIR) spectra shown in Figure 5c indicate the solvation structure of NaFSI-DME electrolytes as a function of NaFSI salt concentration. The characteristic C–O stretching band of pure DME is located at 1110 cm⁻¹ (Figure 5c). Notably, the introduction of NaFSI into DME produced a new peak at 1085 cm⁻¹, which was not observed in pure DME or NaFSI salt. This result indicates that the ion–dipole interactions between the C–O–C moieties and Na⁺ ions affect the C–O–C stretching vibration mode of DME, with DME solvating Na⁺ ions sufficiently to prevent ion pairing. The peak intensity at 1085 cm⁻¹, which arises from coordination between C–O–C moieties and Na⁺ ions, gradually increased as a function of NaFSI salt concentration. The structure of solvated DME interacting with Na⁺ is displayed in the inset of Figure 5c.^{47,48} A comparison of the relative fraction of solvated and free DME, and FSI⁻ anion participating in the solvation structure of Na⁺ cation revealed that the solvation structure such as

$\text{Na}^+(\text{DME})_{1-x}(\text{FSI})_x$ is produced in NaFSI-DME electrolytes and at >2 M NaFSI the contribution of FSI⁻ anion in this solvation structure becomes greater (Figure 7). The oxidation durability of NaFSI-DME electrolytes on an Al working electrode, which is used as the current collector for cathode materials in Na metal batteries, was investigated at a scan rate of 1 mV s^{-1} , which was applied to exclude the effects of polarization resistance on the anodic limit of electrolytes (Figure 5d). 1 M NaPF₆-EC/PC exhibits no appreciable anodic current up to 5.0 V versus Na/Na⁺. Although the anodic current began to increase near 5.0 V, there was no significant current even at 5.5 V. In contrast, conventional dilute 1 M NaFSI-DME displays a sudden increase in the anodic current near 4.0 V, indicating a relatively narrow window of electrochemical stability compared with 1 M NaPF₆-EC/PC. In the case of 1 M NaPF₆-DME, a significant oxidation current was not induced up to around 5.0 V versus Na/Na⁺. Interestingly, the anodic limit of 1 M NaFSI-EC/PC was analogous with that of 1 M NaFSI-DME. It is obvious that FSI⁻ anions dissociated in organic solvents such as DME and EC/PC are not electrochemically stable on an Al working electrode in the high potential region over 4.0 V. Indeed, many pits were observed on the Al surface produced by Al corrosion in 1 M NaFSI-DME (Figure 8b). It was reported that Cl⁻ impurities in the neat salt corrode Al and FSI⁻ anions cause SS corrosion in the high potential region^{46,49} The anodic limits of NaFSI-containing electrolytes can be lowered owing to these characteristics of FSI-based salts. Surprisingly, superior oxidative stability was achieved in more concentrated NaFSI-DME electrolytes. In particular, ultraconcentrated 5 M NaFSI-DME, with the lowest ionic conductivity of 0.584 mS cm^{-1} , showed a slight increase in the anodic current at around 4.0 V on an Al working electrode, but produced no considerable anodic current up to 4.9 V (Figure 5b, d). Moreover, the morphology of the Al surface after the linear sweep voltammetry (LSV) measurements in 5 M NaFSI-DME was nearly identical to that of the pristine Al electrode (Figure 8a, c).

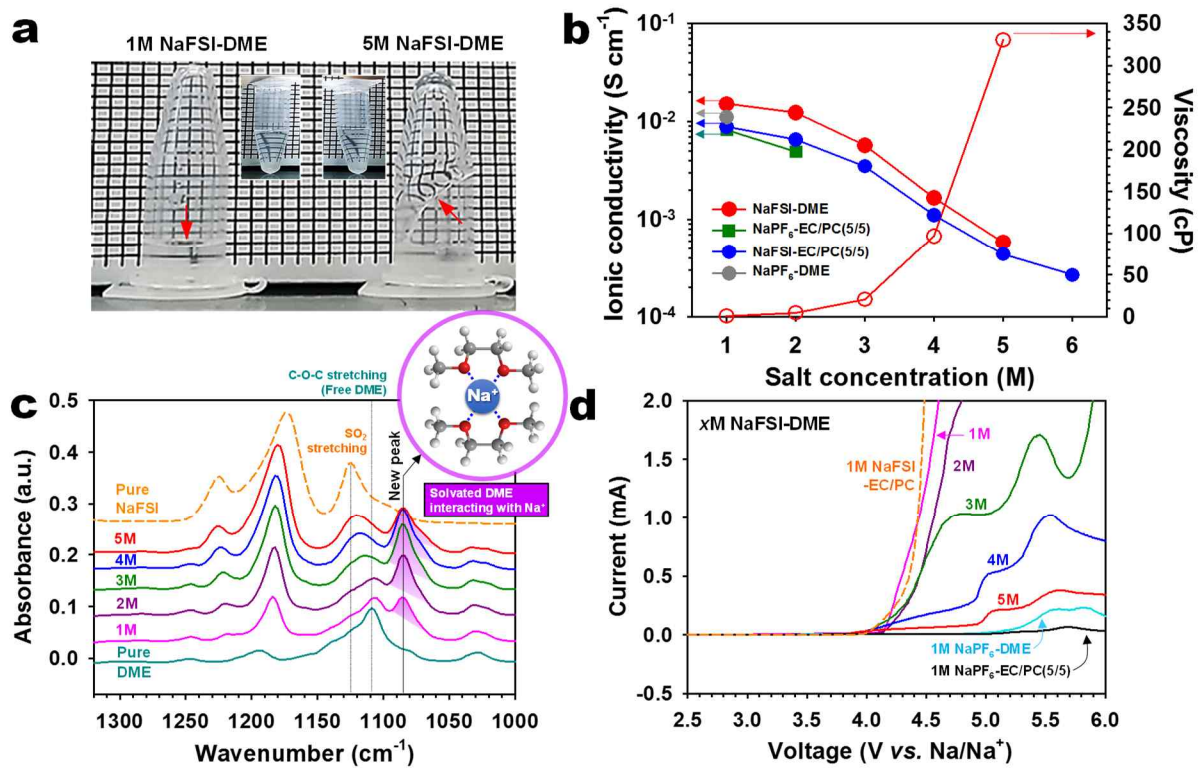


Figure 5. (a) Photograph of 1 and 5 M NaFSI-DME in Eppendorf tubes. (b) Ionic conductivity of x M NaFSI-DME, x M NaPF₆-EC/PC (5/5), x M NaFSI-EC/PC, and 1 M NaPF₆-DME, and viscosity of x M NaFSI-DME at room temperature. (c) FTIR spectra of x M NaFSI-DME ($x = 0, 1, 2, 3, 4,$ and 5) and pure NaFSI salt. (d) Anodic limits of conventional dilute and highly concentrated electrolytes on an Al working electrode at a scan rate of 1 mV s^{-1} .

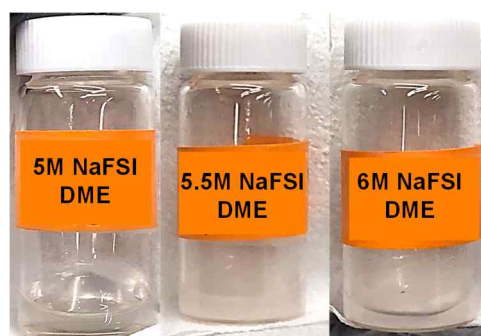


Figure 6. Photograph showing the solubility limit of NaFSI in DME solvent.

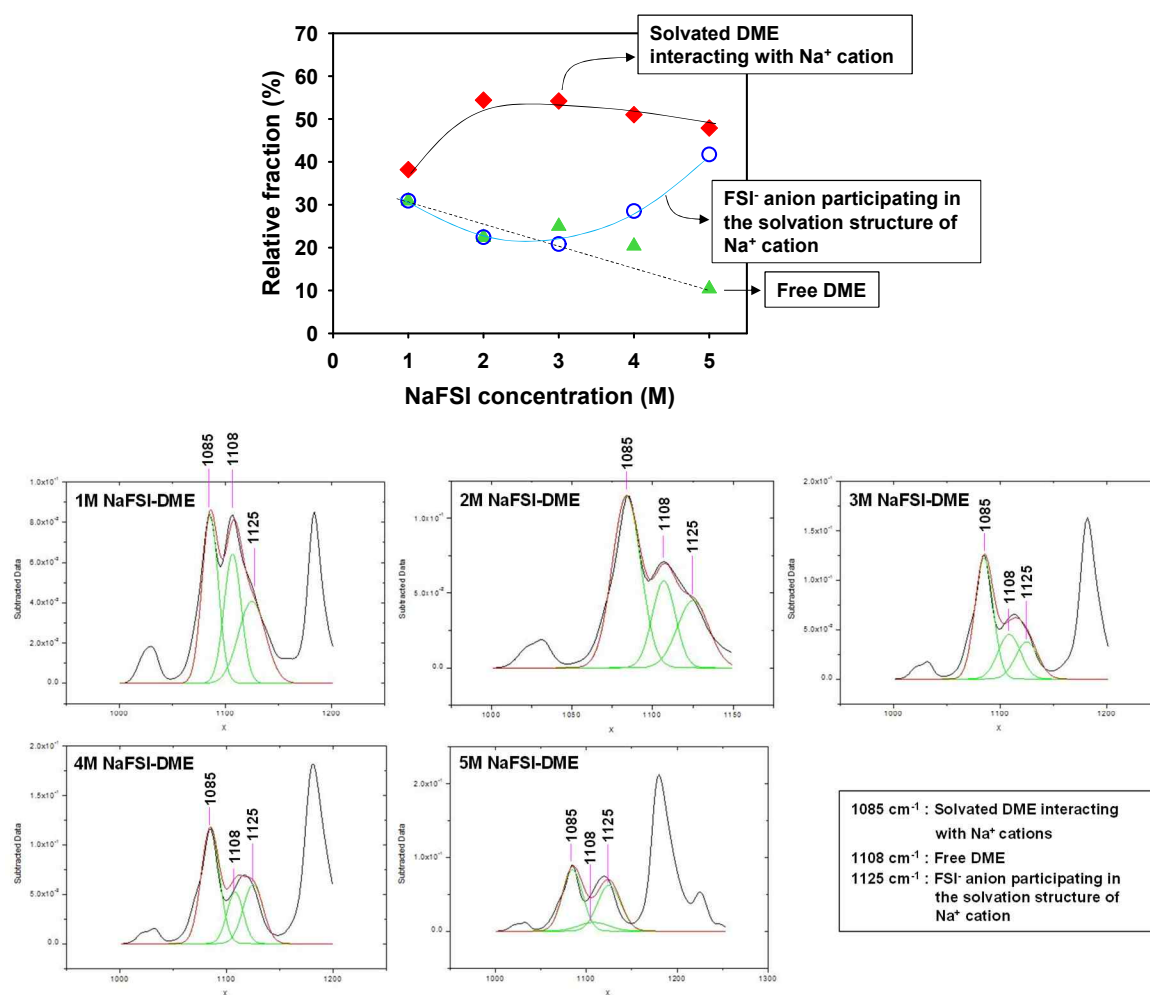


Figure 7. Relative fraction of solvated and free DME, and FSI⁻ anion participating in the solvation of Na⁺ cation as a function of the NaFSI salt concentration (Top). FT-IR peak fitting was performed to calculate the relative fraction of three peaks (Bottom).

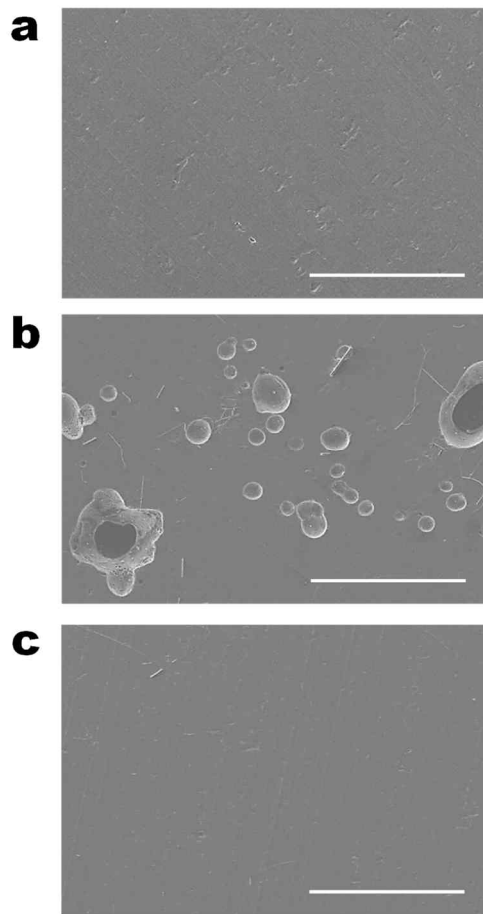


Figure 8. SEM images of (a) pristine Al and Al surfaces after LSV measurements in (b) 1 M NaFSI-DME and (c) 5 M NaFSI-DME (NaFSI : DME = 1.06 : 1 mole ratio) (scale bar: 100 μm).

3.2 Three mechanisms of improved oxidation durability of 5M NaFSI-DME

This improved oxidation durability can be explained by the following three mechanisms. First, the lack of free (uncoordinated) DME hardly dissolves Al–Cl or Al–FSI complexes formed on the Al electrode. Since Al–Cl or Al–FSI complexes on the Al electrode can act as a protective layer against Al corrosion in non-aqueous electrolytes at high voltages, the dissolution of these complexes into the electrolyte is undesirable.³⁷ 5M NaFSI-DME exhibited stronger peak intensity corresponding to S-F of FSI⁻ anion at 686.5 eV and Al-FSI complex at 76 eV compared with 1M NaFSI-DME. From this result, we speculate that the Al-FSI complexes formed in ultraconcentrated 5M NaFSI-DME are not dissolved into the electrolyte and can act as a protective layer against Al corrosion (Figure 9). Second, the oxidative decomposition of solvents is mitigated by the decrease of their highest occupied molecular orbital (HOMO) energy levels. The Watanabe group demonstrated that ethers with relatively strong Lewis basicity readily donate their oxygen lone pair electrons to cations, and these solvated (coordinated) ethers have lower HOMO energy levels than free (uncoordinated) ethers.⁵⁰ Finally, it is noteworthy that unwanted reactions between free organic solvents and a highly reactive Na metal electrode can generate unstable by-products, which may promote the oxidative decomposition of the electrolyte at a cathode charged to a high voltage of 4.2 V vs. Na/Na⁺.¹⁰ In Figure 10, a noticeable feature of the Na metal electrode after stored in 1 M NaFSI-DME with low anodic limit of around 4.1 V for 5 days is the significant color change of the Na metal. This result suggests that conventional dilute 1M NaFSI-DME undergoes severe decomposition at the Na metal. On contrary, there was no discernible color change of the Na metal stored in 5 M NaFSI-DME. This is a clear evidence for low decomposition tendency of 5 M NaFSI-DME at the Na metal electrode. To confirm the oxidation stability of NaFSI-DME electrolytes without Al corrosion, anodic limits on a Pt working electrode were measured (Figure 11). Clearly, ultraconcentrated 5 M NaFSI-DME electrolyte exhibited superior anodic stability on a Pt electrode compared with conventional dilute 1M NaFSI-DME electrolyte. In case of 5 M NaFSI-DME, no appreciable anodic current appeared up to 4.7 V vs. Na/Na⁺ and gradual increase of the anodic current was observed at around 4.7 V on a Pt electrode. On the other hand, 1M NaFSI-DME started to oxidize at around 4.1 V vs. Na/Na⁺ and eventually produced considerable oxidation current on a Pt electrode. Since 5M NaFSI-DME led to the formation of suitable passivation layer inhibiting the Al corrosion and electrolyte decomposition on an Al electrode, it is thought that this ultraconcentrated electrolyte did not produce significant oxidation current up to 5.0 V vs. Na/Na⁺. A comparison of LSV results of 5M NaFSI-DME on Al and Pt electrode clearly shows that drastically reduced oxidation current of 5M NaFSI-DME on an Al electrode at high voltages of greater than 5.0 V is mostly due to the formation of the Al-FSI complexes. This formed Al-FSI complexes may be hardly soluble in superconcentrated 5M NaFSI-

DME and thereby can act as a as passivation layers. From these results, the superior oxidation stability of ultraconcentrated 5 M NaFSI-DME is thought to be ascribed to the formation of a protective layer, such as Al–Cl or Al–FSI complexes, solvated DME with a lower HOMO energy level than free DME, and minimal free DME, which minimizes undesirable interactions with the highly reactive Na metal electrode.

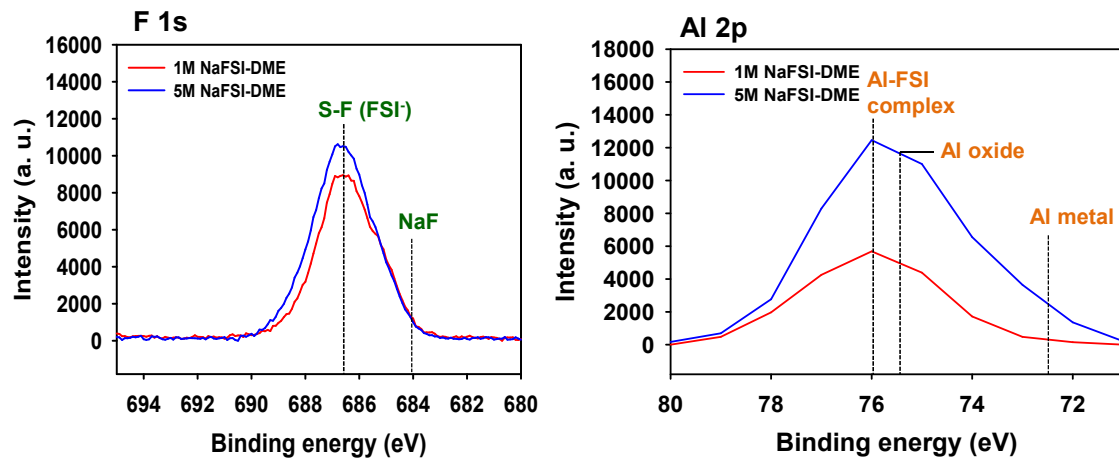


Figure 9. F 1s and Al 2p XPS spectra of Al electrodes after the LSV measurements.

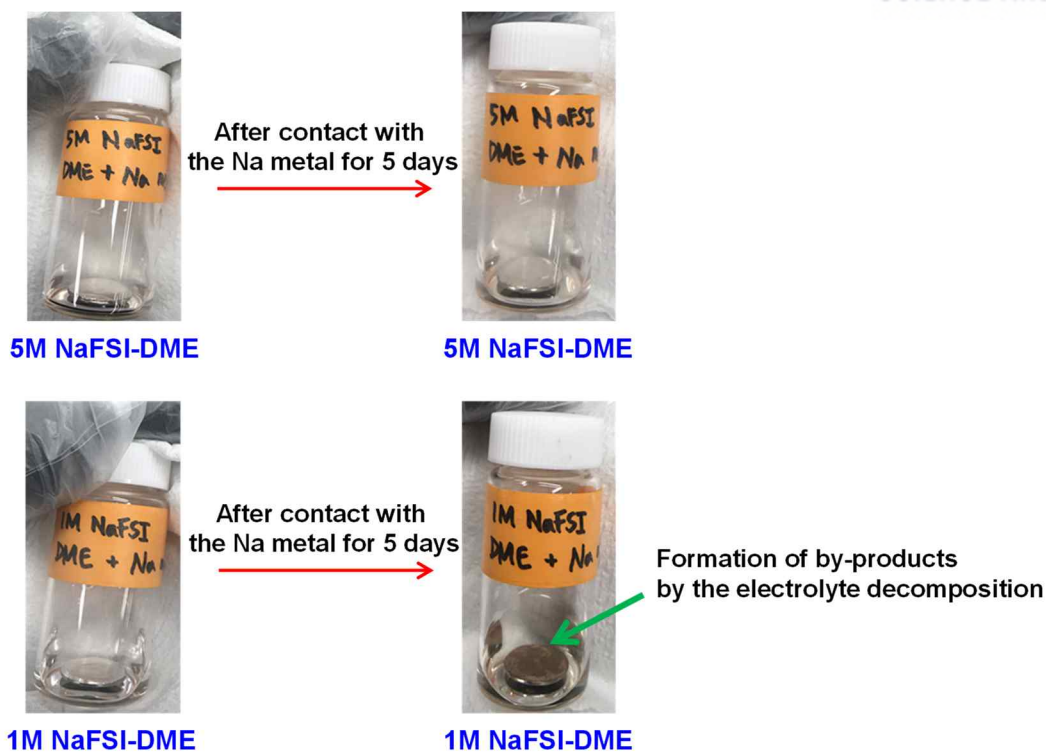


Figure 10. Photograph of Na metal electrodes after contact with 1M NaFSI-DME or 5M NaFSI-DME for 5 days.

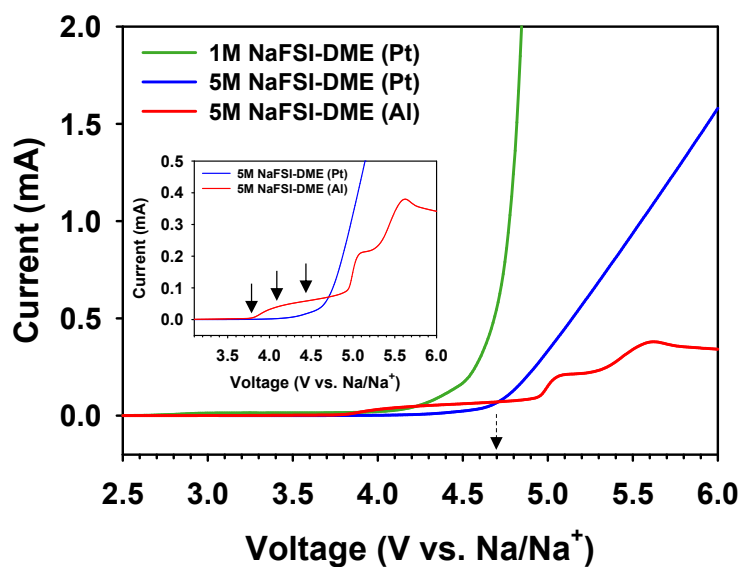


Figure 11. Anodic limits of 1M NaFSI-DME and 5M NaFSI-DME on a Pt electrode at a scan rate of 1 mV s^{-1} . The inset displays the enlarged LSV data for the comparison of anodic limits of 5M NaFSI-DME on Al and Pt electrode. The disc-type Pt electrode (area= 1.77 cm^2) was used as a working electrode.

3.3 Electrochemical performances of Na/SS cells and analysis

A comparison of the voltage profiles for initial Na plating/stripping in coin-type Na/SS cells with electrolytes of various salt concentrations is shown in Figure 12a and 12b. During the first cathodic scan, Na stripping from the Na metal electrode occurs, while the Na metal plates onto the SS working electrode. The overpotential at the beginning of the first cathodic scan of Na/SS cells gradually increased with increasing NaFSI concentration in DME. This phenomenon is mostly due to the high viscosity of concentrated NaFSI-DME electrolytes (Figure 5b). No Na stripping occurred in dilute 1 and 2 M NaFSI-DME electrolytes. However, 1 M NaPF₆-EC/PC and 1 M NaFSI-EC/PC allowed Na stripping from the Na deposits on the SS working electrode, with initial Coulombic efficiencies (ICEs) of 31.1% and 23.6%, respectively (Figure 12a). More concentrated NaFSI-DME electrolytes led to substantially improved ICEs for Na plating/stripping on the SS working electrode. Notably, the highest ICE of 72.7% was achieved in the ultraconcentrated 5 M NaFSI-DME electrolyte. The large polarization of approximately -200 mV versus Na/Na⁺ observed with the 5 M NaFSI-DME electrolyte during the first cathodic scan disappeared after the 2nd cycle and a low polarization of about -10 mV was retained at a rate of C/10 over 100 cycles (Figure 12b). Moreover, with the 5 M NaFSI-DME electrolyte, a very high Coulombic efficiency of 99.3% was attained for the 120th cycle at a rate of C/10, despite the low ionic conductivity of this electrolyte (Figure 12c). Although Na plating/stripping initially occurred in 1 M NaPF₆-EC/PC, the Coulombic efficiency sharply declined to ~10% during cycling (Figure 12c). In the case of 3 M NaFSI-DME, Na plating/stripping in the Na/SS cell took place for only 4 cycles. The use of high NaFSI salt concentration of 6 M in EC/PC (5/5) did not prevent rapid fading of the Coulombic efficiency for Na plating/stripping. This result suggests that the cycling stability of Na/SS cells is greatly affected by the solvent in the highly concentrated electrolyte, and DME is a suitable solvent that ensures reversible Na plating/stripping on the SS working electrode. Interestingly, the incorporation of 1 wt% FEC, which has been widely used as an effective additive for the formation of an SEI on the anode, leads to a discernibly reduced and unstable Coulombic efficiency for Na plating/stripping at a high rate of 1 C in the Na/SS cell with 5 M NaFSI-DME compared with the cell with the FEC-free electrolyte (Figure 13). It is obvious that the formulation of FEC with the ultraconcentrated 5 M NaFSI-DME electrolyte is detrimental to the cycling performance of Na/SS cells because of the resistive NaF formation by the FEC decomposition.²² On the other hand, it is thought that 5 M NaFSI-DME without FEC produces a desirable interfacial structure, allowing highly reversible Na plating/stripping on the SS working electrode. This finding reveals that NaF formed by FEC decomposition acts as a resistive layer for Na plating/stripping in the ultraconcentrated 5 M NaFSI-DME electrolyte.^{17,22} We surmise that minimal amount of free (uncoordinated) DME in the ultraconcentrated 5 M NaFSI-DME electrolyte minimizes

the formation of a resistive SEI layer via interaction of the electrolyte components with reactive Na metal. The impact of ultraconcentrated 5 M NaFSI-DME on the cycling stability at high C rates is shown in Figure 12d. The use of the 5 M NaFSI-DME electrolyte clearly results in a drastically enhanced rate capability compared with the conventional dilute 1 M NaPF₆-EC/PC (5/5) electrolyte. Moreover, a superior Coulombic efficiency is maintained with the 5 M NaFSI-DME electrolyte as a function of the applied C rate, with a Coulombic efficiency of 93.8% at a high rate of 2 C (corresponding to 1.12 mA cm⁻²) at 30 °C. This is likely because the supply of Na ions without the dendritic Na formation was realized by highly viscous 5 M NaFSI-DME. However, the Coulombic efficiency of the Na/SS cells with the conventional dilute 1 M NaPF₆-EC/PC (5/5) electrolyte rapidly fades. The characteristics of the surface layer formed on the electrode are one of the key factors that affects the kinetics and reversibility of the Na plating/stripping process. The formation of an unstable SEI through unavoidable interaction between free organic solvents and reactive Na metal deteriorates the Na metal–electrolyte interface, impeding the Na metal plating/stripping kinetics and eventually, the cell is disabled. Further evidence for the outstanding characteristics of ultraconcentrated 5 M NaFSI-DME as an electrolyte is given by the comparison of Na metal plated on a Cu substrate in 1 M NaPF₆-EC/PC, 1 M NaFSI-DME, and ultraconcentrated 5 M NaFSI-DME (Figure 12e).

Clearly, non-uniform Na metal plating was obtained with 1 M NaPF₆-EC/PC and the plated metal does not have the characteristic silver color of Na metal. This result implies that 1 M NaPF₆-EC/PC severely decomposes during the Na plating process and the Cu substrate is seemingly covered with black-colored electrolyte decomposition products.

Clear evidence for the decomposition of 1 M NaPF₆-EC/PC is given in Figure 14. It is notable that very rough surface morphology was observed on the electrochemically deposited Na metal obtained from 1 M NaPF₆-EC/PC. A relatively strong carbon (C) signal produced by the decomposition of EC and PC solvents appeared for the Na deposit on the Cu substrate with 1 M NaPF₆-EC/PC (5/5) compared with 5 M NaFSI-DME electrolyte. The appearance of P and F signals implies that the NaPF₆ decomposition takes place during the Na deposition in 1 M NaPF₆-EC/PC. In the case of 1 M NaFSI-DME, Na metal plating mostly occurred near the center of the Cu substrate and dark-brown-colored by-products produced by decomposition of this electrolyte during the plating process were observed on the edge of the substrate. Surprisingly, the ultraconcentrated 5 M NaFSI-DME electrolyte allowed uniform Na metal plating across the entire surface of the Cu substrate, and the color of Na metal plated on the Cu substrate was quite similar to that of the pristine Na metal. This uniform Na metal plating was also confirmed by the SEM image of Figure 14. Importantly, the EDS result of Figure 14 manifests that the DME decomposition to produce the C signal is mitigated in the ultraconcentrated 5 M NaFSI-DME electrolyte. From these results, the interfacial characteristics

between Na metal and the electrolyte is believed to be the important factor affecting the rate capability of the Na/SS cells.

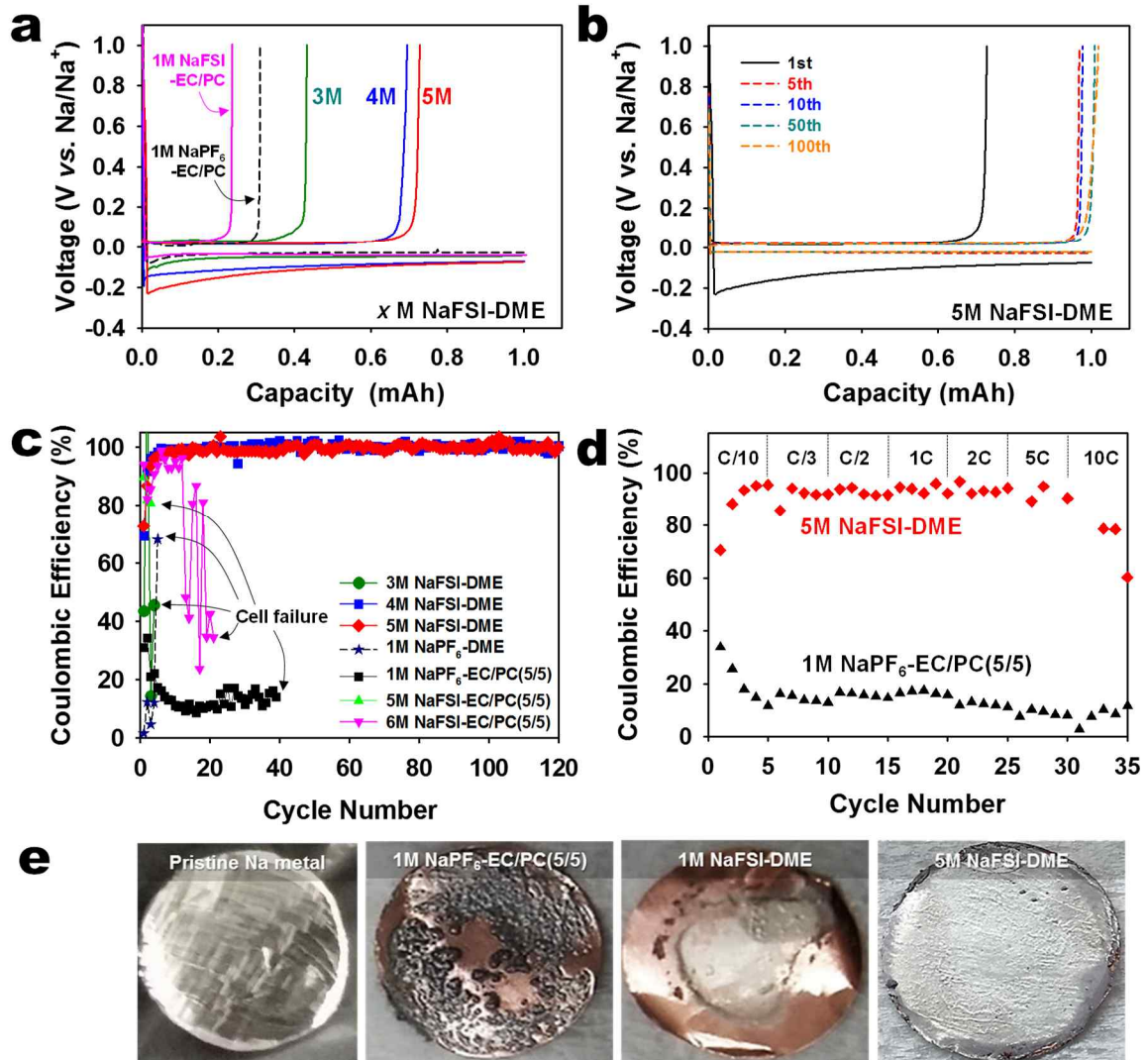


Figure 12. (a) Voltage profiles for initial Na plating/stripping in the coin-type Na/SS cells at a rate of C/10 (0.056 mA cm^{-2}). (b) Voltage profiles of 5 M NaFSI-DME during the 1st, 5th, 10th, 50th, and 100th cycles at a rate of C/10. (c) Coulombic efficiency for Na plating/stripping in Na/SS cells. (d) Coulombic efficiency of Na/SS cells with 5 M NaFSI-DME and 1 M NaPF₆ EC/PC (5/5) at various C rates. (e) Photographs of a pristine Na metal electrode and Cu substrates after the initial Na plating at a rate of C/10. The utilized capacity of the Na metal electrode was 5.0 mAh.

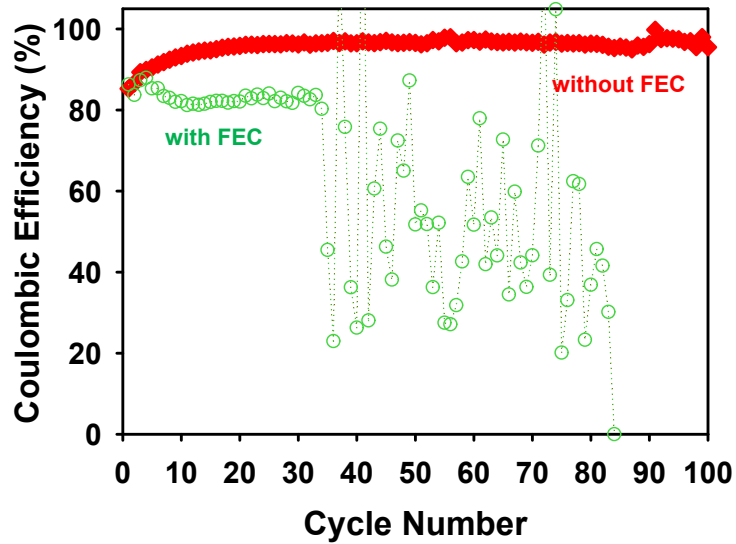


Figure 13. Coulombic efficiency of Na/SS cells during 100 cycles at a 1 C rate (corresponding to a current density of 0.56 mA cm^{-2}) after precycling at a C/10 rate. 5 M NaFSI-DME with and without 1 wt% FEC was used as the electrolyte. The utilized capacity of the Na metal electrode was 1.0 mAh.

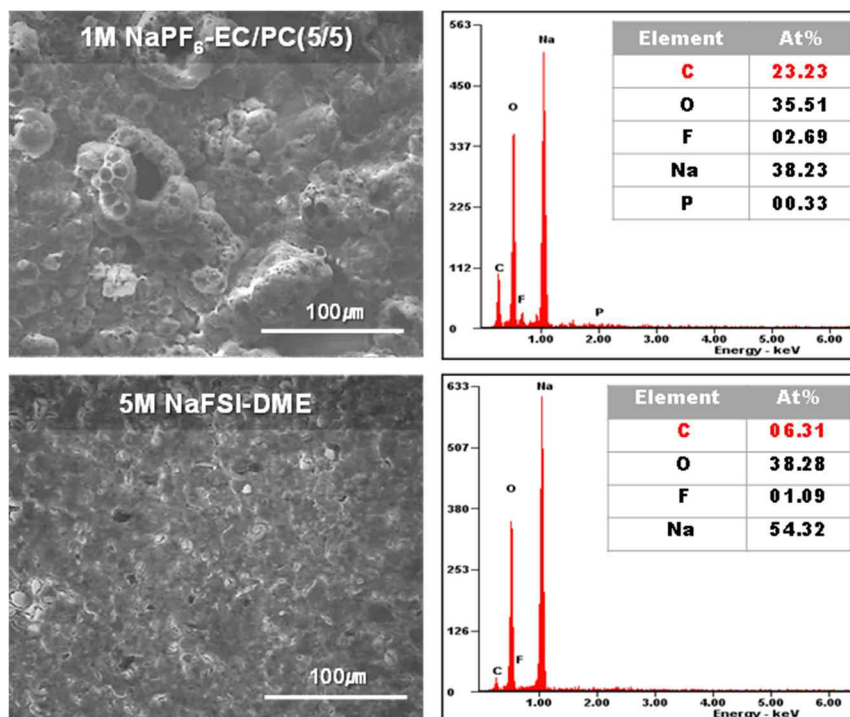


Figure 14. A comparison of SEM images and EDS patterns of Na deposit on Cu substrates with 1 M $\text{NaPF}_6\text{-EC/PC (5/5)}$ and 5 M NaFSI-DME after the initial Na plating at a rate of C/10. The utilized capacity of the Na metal electrode was 5.0 mAh.

3.4 Electrochemical performances of Na/Na symmetric cells and analysis

The voltage profiles at current densities of $0.0014 \text{ mA cm}^{-2}$ and $0.0028 \text{ mA cm}^{-2}$ during galvanostatic cycling of Na/Na symmetric cells with a 1 M NaPF₆-EC/PC (5/5), 1 M NaFSI-DME, or 5 M NaFSI-DME electrolyte are presented in Figure 15. The initial steep and large overpotential of the Na/Na symmetric cells with a 1 M NaPF₆-EC/PC (5/5) or 5 M NaFSI-DME electrolyte is thought to be a result of an interfacial structure that impedes initiation of Na stripping from the Na metal electrode and Na deposition on the counter Na metal electrode during the first cathodic scan at a current density of $0.0014 \text{ mA cm}^{-2}$. The dilute conventional electrolyte, 1 M NaPF₆-EC/PC (5/5), showed a relatively large overpotential between the two Na electrodes during 600 cycles at a current density of $0.0028 \text{ mA cm}^{-2}$ with the time cut-off condition of 0.5 h. This indicates that the electrolyte forms a resistive SEI layer that causes the overpotential for the Na plating/stripping process on the Na metal electrode. Although 1 M NaFSI-DME showed a greatly reduced overpotential barrier for Na metal plating/stripping during the first cathodic scan, its overpotential gradually increased during cycling, becoming larger than that of the ultraconcentrated 5 M NaFSI-DME electrolyte (Figure 15a). Importantly, a highly stable voltage profile and low overpotential for Na metal plating/stripping on the Na metal electrode were observed with the ultraconcentrated 5 M NaFSI-DME electrolyte after 600 cycles at a current density of $0.0028 \text{ mA cm}^{-2}$. The differences in the overpotentials for Na metal plating/stripping on the Na metal electrode are more clearly shown in Figure 15b. For instance, 1 M NaPF₆-EC/PC (5/5) showed an overpotential of -18.3 mV for the cathodic scan (Na plating on the Na counter electrode), whereas a low overpotential of -4.6 mV was obtained with the 5 M NaFSI-DME electrolyte. This finding indicates that the interfacial structure formed in the 5 M NaFSI-DME electrolyte effectively assists Na migration to the Na metal electrode and allows reversible Na metal stripping/plating in the Na/Na symmetric cell.

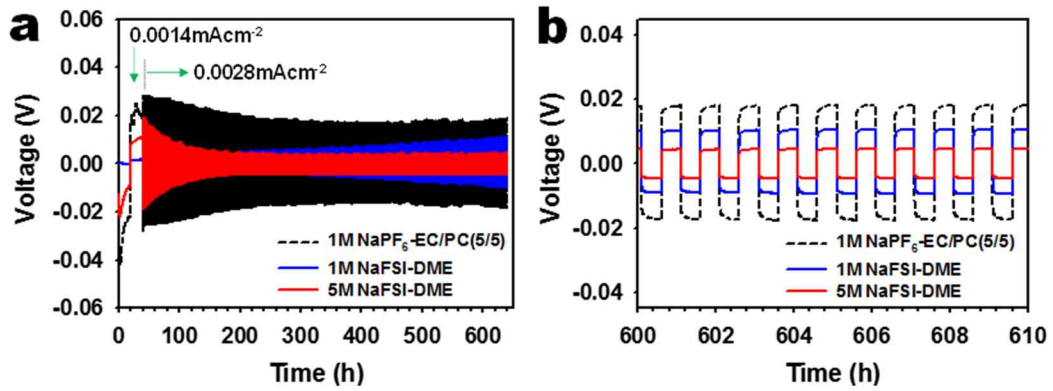


Figure 15. (a) Galvanostatic cycling of Na/Na symmetric cells during 600 cycles with the time cut-off condition of 0.5 h at a current density of 0.0028 mA cm⁻² after precycling at a current density of 0.0014 mA cm⁻². (b) Enlarged region showing the voltage profiles for the 561st to 570th cycles.

3.5 Electrochemical performances of Na/Cathode cells and analysis

Figure 16a shows two voltage plateaus near 2.9 V and 3.2 V vs. Na/Na⁺, which corresponds to the reversible extraction of Na ions from the Na₄Fe₃(PO₄)₂(P₂O₇) cathode during the charge process of precycling. Na/Na₄Fe₃(PO₄)₂(P₂O₇) cells with 1 M NaPF₆-EC/PC (5/5) and 5 M NaFSI-DME delivered the discharge capacities of 111.4 mAh g⁻¹ and 116.2 mAh g⁻¹ during precycling, respectively. When this cathode was cycled in 1 M NaPF₆-EC/PC (5/5), a low Coulombic efficiency of ca. 96% was achieved over 300 cycles at a rate of C/2 (Figure 16c). In addition, a relatively large voltage hysteresis was observed for the Na/Na₄Fe₃(PO₄)₂(P₂O₇) cell with 1 M NaPF₆-EC/PC (5/5) during cycling (Figure 17a). In contrast, this cathode with 5 M NaFSI-DME exhibits a slightly higher charge plateau and a lower discharge plateau due to the polarization caused by the high viscosity of the ultraconcentrated electrolyte (Figure 16a). Nevertheless, the Na/Na₄Fe₃(PO₄)₂(P₂O₇) cell with 5 M NaFSI-DME delivers a higher discharge capacity (109.4 mAh g⁻¹) than that with 1 M NaPF₆-EC/PC (5/5) (95.3 mAh g⁻¹) during the 300th cycle and displays outstanding cycling stability with a high Coulombic efficiency of ca. 99% over 300 cycles at a rate of C/2 (Figure 16b and 16c). In addition, extremely stable charge and discharge profiles without noticeable capacity loss and discernibly reduced voltage hysteresis over 300 cycles were achieved with ultraconcentrated 5 M NaFSI-DME (Figure 17b). This finding reveals that the low ionic conductivity of the ultraconcentrated 5 M NaFSI-DME electrolyte does not hinder the electrochemical reactions of the Na₄Fe₃(PO₄)₂(P₂O₇) cathode. Cells with lower concentrations of NaFSI in DME (1 M and 4 M) showed severe overcharge behaviors for the first desodiation (charge) of the Na₄Fe₃(PO₄)₂(P₂O₇) cathode during precycling and the sodiation (discharge) process did not proceed (Figure 18). This result is in good agreement with the findings that 1 and 4 M NaFSI-DME electrolytes are electrochemically unstable at high voltages (>4.0 V versus Na/Na⁺) and that the concentrated 4 M NaFSI-DME electrolyte has relatively inferior oxidation durability compared with ultraconcentrated 5 M NaFSI-DME (Figure 5d). Therefore, it is thought that less concentrated NaFSI-DME electrolytes are not suitable for use with the Na₄Fe₃(PO₄)₂(P₂O₇) cathode because of their severe electrochemical decomposition behavior at high voltages of around 4.0 V versus Na/Na⁺. The cell with the 1 M NaFSI-DME electrolyte exhibited considerable overcharging with an increased length of the voltage plateau at around 3.2 V versus Na/Na⁺ and caused a significant color change of the Na metal electrode and a glass fiber filter (GFF) separator (Figure 18). The cell with the more concentrated 4 M NaFSI-DME electrolyte, which did not exhibit overcharging at 3.2 V versus Na/Na⁺, showed a similar charge voltage profile up to 4.0 V. After reaching 4.0 V versus Na/Na⁺, overcharging with a long voltage plateau at around 3.9 V was observed in the Na/Na₄Fe₃(PO₄)₂(P₂O₇) cell with 4 M NaFSI-DME. The excellent electrochemical performances of ultraconcentrated 5 M NaFSI-DME were observed not only with the phosphate-

based cathode, $\text{Na}_4\text{Fe}_3(\text{PO}_4)_2(\text{P}_2\text{O}_7)$, but also with a layered oxide-based cathode, P2- $\text{Na}_{0.7}(\text{Fe}_{0.5}\text{Mn}_{0.5})\text{O}_2$ having a wide operating potential range between 1.5 V and 4.3 V vs. Na/Na^+ . $\text{Na}_{0.7}(\text{Fe}_{0.5}\text{Mn}_{0.5})\text{O}_2$ has been considered one of promising cathode materials owing to the use of inexpensive Fe and Mn and its high theoretical capacity (259 mAh g^{-1} for the extraction of 1 Na atom from the cathode).⁴⁵ $\text{Na}_{0.7}(\text{Fe}_{0.5}\text{Mn}_{0.5})\text{O}_2$ was obtained through a conventional solid state synthesis, and no impurity peaks were observed in the XRD pattern shown in Figure 19. Figure 16d and 16e show the charge–discharge profiles during precycling and the discharge capacity retention of P2- $\text{Na}_{0.7}(\text{Fe}_{0.5}\text{Mn}_{0.5})\text{O}_2$ after the precycle, respectively.⁴⁴ The $\text{Na}_{0.7}(\text{Fe}_{0.5}\text{Mn}_{0.5})\text{O}_2$ cathode with 1 M $\text{NaPF}_6\text{-EC/PC}$ (5/5) delivered a charge capacity of 113.4 mAh g^{-1} (corresponding to the extraction of 0.44 Na atoms from the cathode) during precycling at a rate of C/20 (Figure 16d). The cathode with the ultraconcentrated 5 M NaFSI-DME exhibited a slightly higher charge capacity of 137.2 mAh g^{-1} (corresponding to the extraction of 0.53 Na atoms from the cathode). For the precycling, the discharge capacities are larger than the charge capacities because of the Na deficiency in $\text{Na}_{0.7}(\text{Fe}_{0.5}\text{Mn}_{0.5})\text{O}_2$. (165.3 mAh g^{-1} and 175.2 mAh g^{-1} for 1 M $\text{NaPF}_6\text{-EC/PC}$ (5/5) and 5 M NaFSI-DME , respectively). More importantly, the discharge capacity retention of the $\text{Na}_{0.7}(\text{Fe}_{0.5}\text{Mn}_{0.5})\text{O}_2$ cathode was greatly improved from 55.9% in 1 M $\text{NaPF}_6\text{-EC/PC}$ (5/5) to 82.1% in 5 M NaFSI-DME after 100 cycles at a rate of C/2 at 30 °C (Figure 16e, Figure 17c and 17d). It is clear that the P2-type $\text{Na}_{0.7}(\text{Fe}_{0.5}\text{Mn}_{0.5})\text{O}_2$ cathode undergoes reversible electrochemical reactions in the ultraconcentrated 5 M NaFSI-DME electrolyte (Figure 16e). Moreover, the $\text{Na}_{0.7}(\text{Fe}_{0.5}\text{Mn}_{0.5})\text{O}_2$ cathode with 5 M NaFSI-DME displayed an improved Coulombic efficiency of close to 99% compared with the Coulombic efficiency of ca. 97% obtained with 1 M $\text{NaPF}_6\text{-EC/PC}$ (5/5) (Figure 16f).

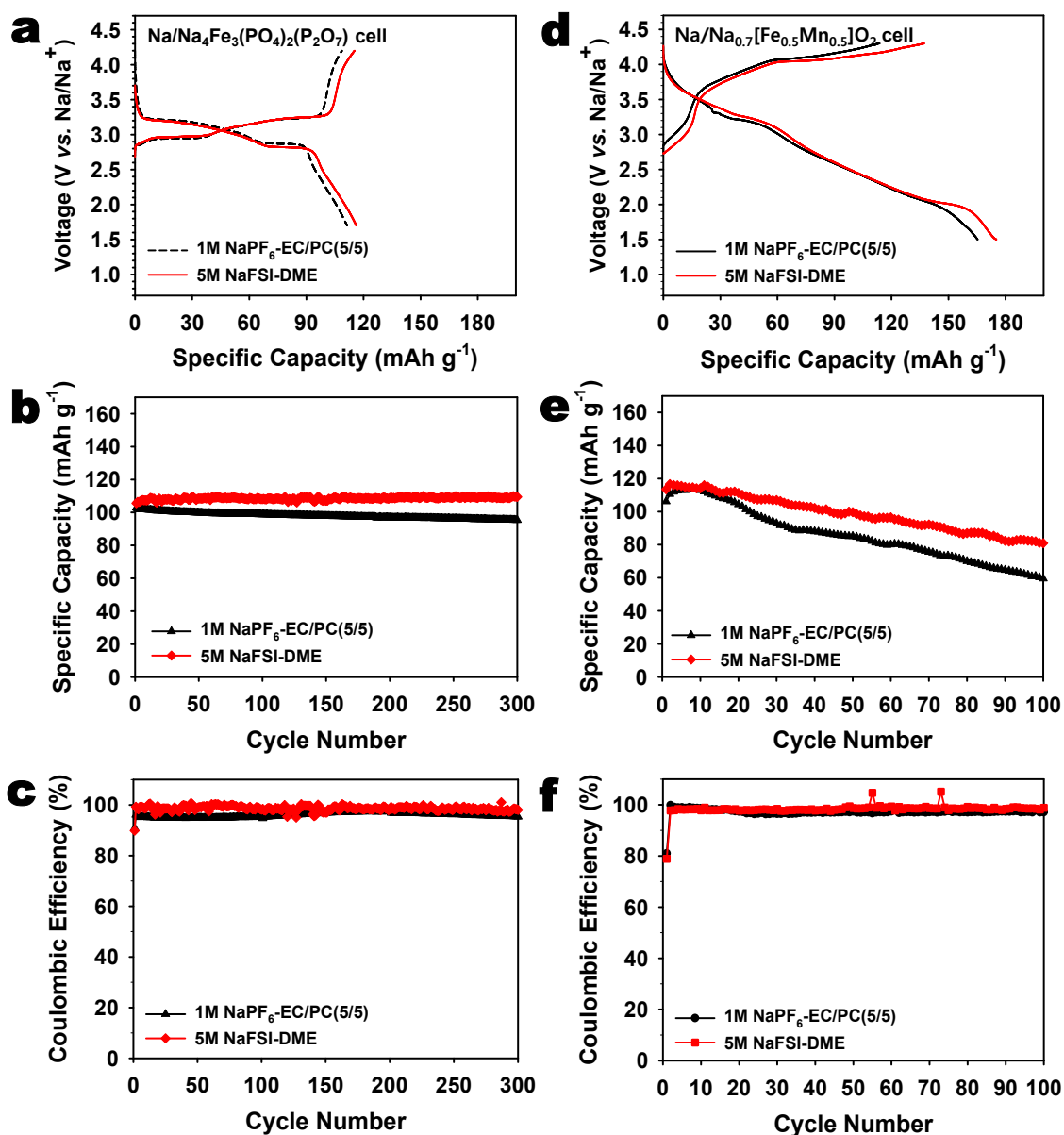


Figure 16. (a) Initial voltage profiles of Na/Na₄Fe₃(PO₄)₂(P₂O₇) full cells at a rate of C/20. (b) Discharge capacity and (c) Coulombic efficiency of Na/Na₄Fe₃(PO₄)₂(P₂O₇) full cells during 300 cycles at a rate of C/2. (d) Initial voltage profiles of Na/Na_{0.7}(Fe_{0.5}Mn_{0.5})O₂ full cells at a rate of C/20. (e) Discharge capacity and (f) Coulombic efficiency of Na/Na_{0.7}(Fe_{0.5}Mn_{0.5})O₂ full cells during 100 cycles at a rate of C/2.

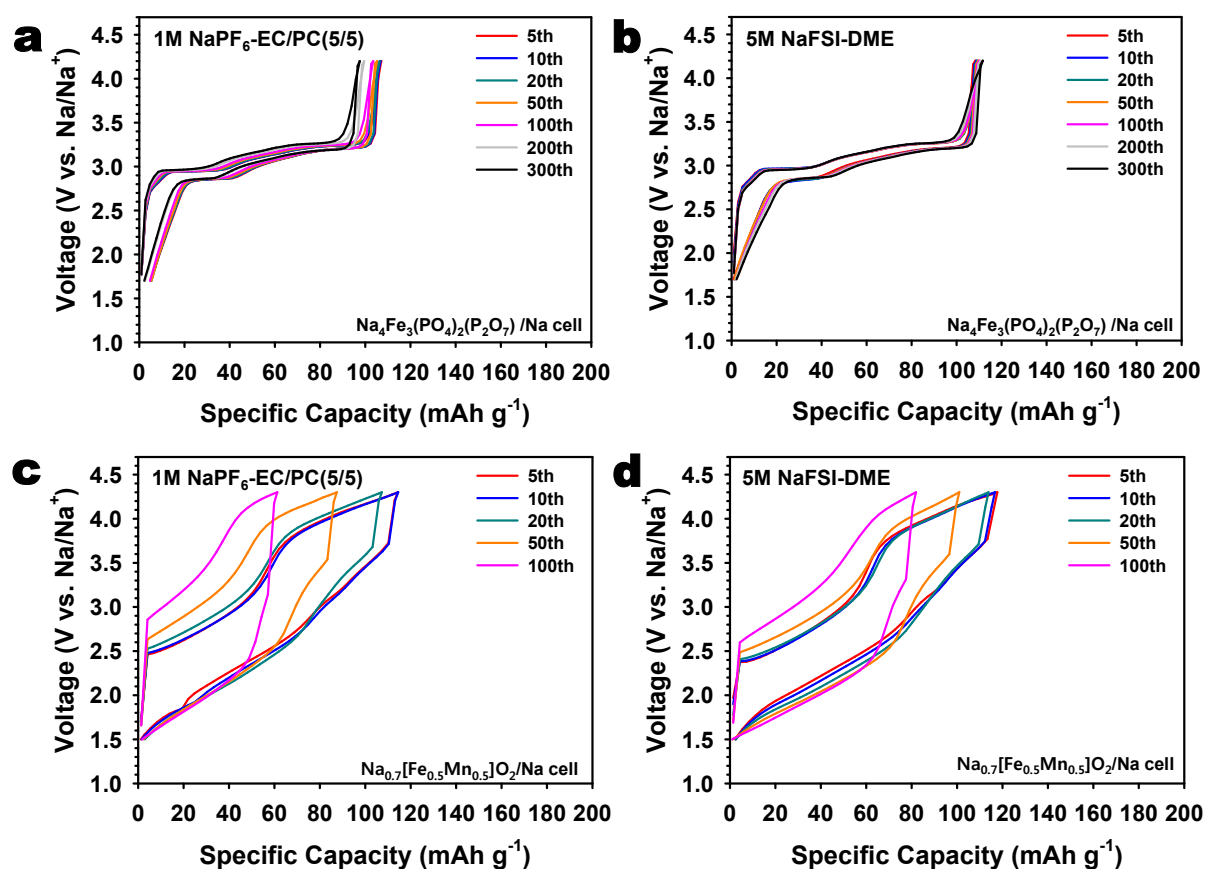


Figure 17. Voltage–capacity profiles of the Na₄Fe₃(PO₄)₂(P₂O₇) cathode during the 5th, 10th, 20th, 50th, and 100th cycles in (a) 1 M NaPF₆-EC/PC (5/5) and (b) 5 M NaFSI-DME at a rate of C/2. Voltage–capacity profiles of the Na_{0.7}(Fe_{0.5}Mn_{0.5})O₂ cathode in (c) 1 M NaPF₆-EC/PC (5/5) and (d) 5 M NaFSI-DME at a rate of C/2.

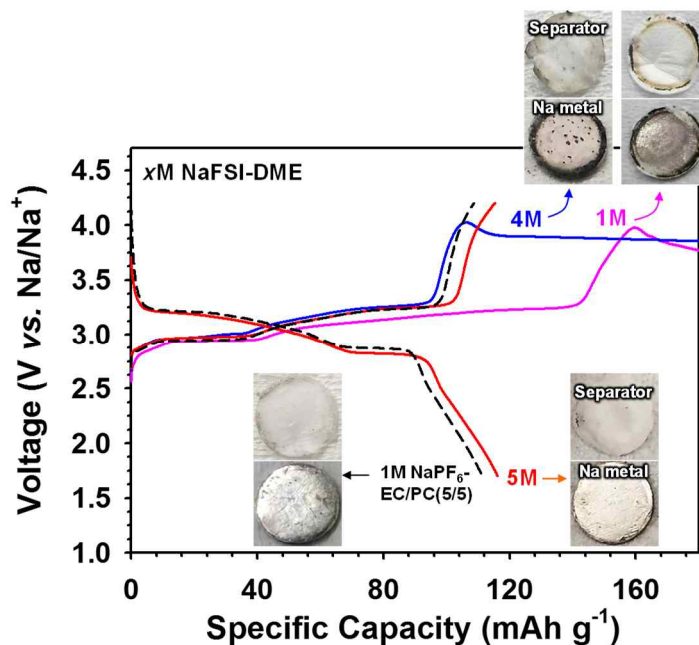


Figure 18. Voltage profiles of the $\text{Na}_4\text{Fe}_3(\text{PO}_4)_2(\text{P}_2\text{O}_7)$ cathode during precycling at a rate of C/20. The inset photographs show Na metal electrodes and GFF separators retrieved from Na/ $\text{Na}_4\text{Fe}_3(\text{PO}_4)_2(\text{P}_2\text{O}_7)$ cells with 1 M, 4 M, or 5 M NaFSI-DME after precycling. For comparison, the voltage profiles of the $\text{Na}_4\text{Fe}_3(\text{PO}_4)_2(\text{P}_2\text{O}_7)$ cathode with 1 M $\text{NaPF}_6\text{-EC/PC (5/5)}$ and photographs of the retrieved Na metal electrodes and GFF separators are included.

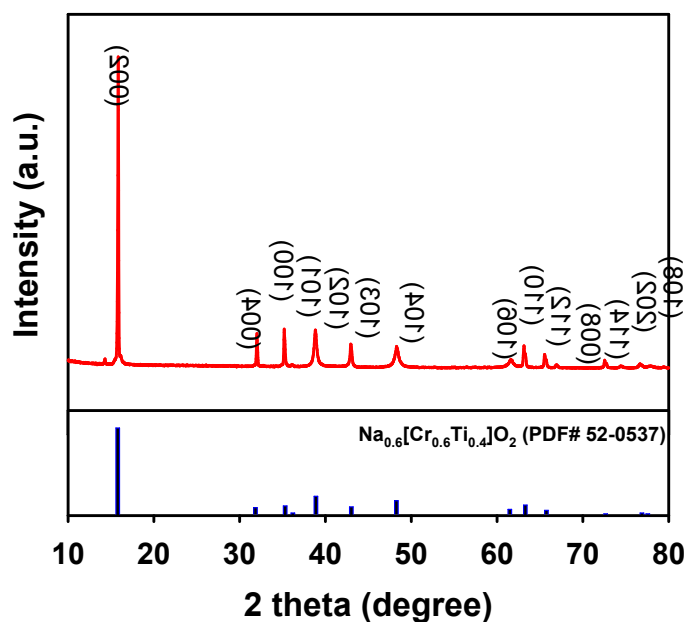


Figure 19. XRD pattern of the synthesized $\text{Na}_{0.7}(\text{Fe}_{0.5}\text{Mn}_{0.5})\text{O}_2$ cathode.

IV. Conclusion

In summary, although sodium metal batteries have attracted considerable attention as promising next-generation rechargeable batteries, especially for large-scale energy storage systems (ESS), there are some issues to solve for commercializing the sodium metal batteries. The first is high reactivity of sodium metal. Owing to the high reactivity, the use of linear carbonates such as dimethyl carbonate (DMC), which are widely used as electrolyte solvents in lithium batteries cannot be used in sodium metal batteries. The second is highly oxidative environment. Since normal hydrogen electrode of sodium-ion redox potential is higher than that of lithium, sodium metal battery has relatively higher oxidative environment. Finding new electrolyte systems that are stable at the Na metal electrode and possess high oxidation durability at high-voltage cathodes is necessary for the development of high-performance Na metal batteries.

Herein, we used new electrolyte system, highly concentrated electrolyte system for sodium metal batteries. We have demonstrated that the ultraconcentrated 5 M NaFSI-DME electrolyte has excellent electrochemical stability toward highly reactive Na metal electrodes, ensures superior reversibility of Na metal plating/stripping in Na/SS cells and Na/Na symmetric cells, and improves the oxidation durability on Al substrates. Furthermore, a noticeable improvement of the cycling performance of high-voltage $\text{Na}_4\text{Fe}_3(\text{PO}_4)_2(\text{P}_2\text{O}_7)$ and $\text{Na}_{0.7}(\text{Fe}_{0.5}\text{Mn}_{0.5})\text{O}_2$ cathodes was achieved in the ultraconcentrated 5 M NaFSI-DME electrolyte. The data obtained in this study allows the design suitable electrolyte systems with the promise of further improvements in the electrochemical performance of Na metal anodes coupled with high-voltage cathodes.

Most contents of this thesis are published in ACS Applied Materials & Interfaces.⁵¹
(DOI: 10.1021/acsami.6b14878)

References

- (1) Yabuuchi, N.; Kubota, K.; Dahbi, M.; Komaba, S. Research Development on Sodium-Ion Batteries. *Chem. Rev.* **2014**, *114*, 11636-11682.
- (2) Ellis, B. L.; Nazar, L. F. Sodium and Sodium-Ion Energy Storage Batteries. *Curr. Opin. Solid State Mater. Sci.* **2012**, *16*, 168-177.
- (3) Palomares, V.; Serras, P.; Villaluenga, I.; Hueso, K. B.; Carretero-Gonzalez, J.; Rojo, T. Na-Ion Batteries, Recent Advances and Present Challenges to Become Low Cost Energy Storage Systems. *Energy Environ. Sci.* **2012**, *5*, 5884-5901.
- (4) Cao, Y.; Xiao, L.; Wang, W.; Choi, D.; Nie, Z.; Yu, J.; Saraf, L. V.; Yang, Z.; Liu, J. Reversible Sodium Ion Insertion in Single Crystalline Manganese Oxide Nanowires with Long Cycle Life. *Adv. Mater.* **2011**, *23*, 3155-3760
- (5) Ha, K.-H.; Woo, S. H.; Mok, D.; Choi, N.-S.; Park, Y.; Oh, S. M.; Kim, Y.; Kim, J.; Lee, J.; Nazar, L. F.; Lee, K. T. $\text{Na}_{4-\alpha}\text{M}_{2+\alpha/2}(\text{P}_2\text{O}_7)_2$ ($2/3 \leq \alpha \leq 7/8$, $\text{M} = \text{Fe}, \text{Fe}_{0.5}\text{Mn}_{0.5}, \text{Mn}$): A Promising Sodium Ion Cathode for Na-ion Batteries. *Adv. Energy Mater.* **2013**, *3*, 770-776.
- (6) Kim, H.; Park, I.; Lee, S.; Kim, H.; Park, K.-Y.; Park, Y.-U.; Kim, H.; Kim, J.; Lim, H.-D.; Yoon, W.-S.; Kang, K. Understanding the Electrochemical Mechanism of the New Iron-Based Mixed-Phosphate $\text{Na}_4\text{Fe}_3(\text{PO}_4)_2(\text{P}_2\text{O}_7)$ in a Na Rechargeable Battery. *Chem. Mater.* **2013**, *25*, 3614-3622.
- (7) Gao, J.; Zhao, P.; Feng, K. $\text{Na}_{2.67}\text{Mn}_{1.67}(\text{MoO}_4)_3$: A 3.45 V Alluaudite-Type Cathode Candidate for Sodium-ion Batteries. *Chem. Mater.* **2017**, *29*, 940-944.
- (8) Lu, J.; Nishimura, S.; Yamada, A. A Fe-rich sodium iron orthophosphate as cathode material for rechargeable batteries. *Electrochem. Commun.* **2017**, *79*, 51-54.
- (9) KLee, R.; Wiatrowski, M.; Aragon, M. J.; Lavela, P.; Ortiz, G. F.; Alcantara, R.; Tirado, J. L.; Improved Surface Stability of $\text{C}+\text{M}_x\text{O}_y@ \text{Na}_3\text{V}_2(\text{PO}_4)_3$ Prepared by Ultrasonic Method as Cathode for Sodium-Ion Batteries. *ACS Appl. Mater. Interfaces*, **2017**, *9*, 1471-1478.

- (10) Chen, M.; Chen, L.; Hu, Z.; Liu, Q.; Zhang, B.; Hu, Y.; Gu, Q.; Wang, J.-L.; Wang, L.-Z.; Guo, X.; Chou, S.-L.; Dou, S.-X. Carbon-Coated $\text{Na}_{3.32}\text{Fe}_{2.34}(\text{P}_2\text{O}_7)_2$ Cathode Material for High-Rate and Long-Life Sodium-Ion Batteries. *Adv. Mater.* **2017**, 1605535.
- (11) Li, Z.-Y.; Gao, R.; Sun, L.; Hu, Z.; Liu, X. Zr-doped P2- $\text{Na}_{0.75}\text{Mn}_{0.55}\text{Ni}_{0.25}\text{Co}_{0.05}\text{Fe}_{0.10}\text{Zr}_{0.05}\text{O}_2$ as high-rate performance cathode material for sodium ion batteries. *Electrochim. Acta* **2017**, 223, 92-99.
- (12) De Iaeduya, J. M.; Otaegui, L.; Del Amo, J. M. L.; Armand, M.; Singh, G. NaN_3 addition, a strategy to overcome the problem of sodium deficiency in P2- $\text{Na}_{0.67}[\text{Fe}_{0.5}\text{Mn}_{0.5}]\text{O}_2$ cathode for sodium-ion battery. *J. Power Sources* **2017**, 337, 197-203.
- (13) Hou, H.; Gan, B.; Gong, Y.; Chen, N.; Sun, C. P2-Type $\text{Na}_{0.67}\text{Ni}_{0.23}\text{Mg}_{0.1}\text{Mn}_{0.67}\text{O}_2$ as a High-Performance Cathode for a Sodium-Ion Battery. *Inorg. Chem.* **2016**, 55, 9033-9037.
- (14) Shiva, K.; Singh, P.; Zhou, W.; Goodenough, J. B. $\text{NaFe}_2\text{PO}_4(\text{SO}_4)_2$: a potential cathode for a Na-ion battery. *Energy Environ. Sci.* **2016**, 9, 3103-3106.
- (15) Kim, Y.; Park, Y.; Choi, A.; Choi, N.-S.; Kim, J.; Lee, J.; Ryu, J. H.; Oh, S. M.; Lee, K. T. An Amorphous Red Phosphorus/Carbon Composite as a Promising Anode Material for Sodium Ion Batteries. *Adv. Mater.* **2013**, 25, 3045-3049.
- (16) Ko, Y. N.; Kang, Y. C. Electrochemical Properties of Ultrafine Sb Nanocrystals Embedded in Carbon Microspheres for Use as Na-Ion Battery Anode Materials. *Chem. Commun.* **2014**, 50, 12322-12324.
- (17) Irisarri, E.; Ponrouch, A.; Palacin, M. R. Review—Hard Carbon Negative Electrode Materials for Sodium-Ion Batteries. *J. Electrochem. Soc.* **2015**, 162, A2476-A2482.
- (18) Wang, G.; Xiong, X.; Lin, Z.; Yang, C.; Lin, Z.; Liu, M. Sb/C composite as a high-performance anode for sodium ion batteries. *Electrochim. Acta* **2017**, 242, 159-164.
- (19) Ou, X.; Yang, C.; Xiong, X.; Zheng, F.; Pan, Q.; Jin, C.; Liu, M.; Huang, K. A New rGO-Overcoated Sb_2Se_3 Nanorods Anode for Na^+ Battery: In Situ X-Ray Diffraction Study on a Live Sodiation/Desodiation Process. *Adv. Funct. Mater.* **2017**, 27, 1606242.

- (20) Jang, J. Y.; Kim, H.; Lee, Y.; Lee, K. T.; Kang, K.; Choi, N.-S. *Electrochem. Commun.* Cyclic carbonate based-electrolytes enhancing the electrochemical performance of $\text{Na}_4\text{Fe}_3(\text{PO}_4)_2(\text{P}_2\text{O}_7)$ cathodes for sodium-ion batteries. **2014**, *44*, 74-77.
- (21) Ponrouch, A.; Monti, D.; Boschini, A.; Steen, B.; Johansson, P.; Palacin, M. R. Non-Aqueous Electrolytes for Sodium-Ion Batteries. *J. Mater. Chem. A* **2015**, *3*, 22-42.
- (22) Jang, J. Y.; Lee, Y.; Kim, Y.; Lee, J.; Lee, S.-M.; Lee, K. T.; Choi, N.-S. Interfacial Architectures Based on a Binary Additive Combination for High-Performance Sn_4P_3 Anodes in Sodium-Ion Batteries. *J. Mater. Chem. A* **2015**, *3*, 8332-8338.
- (23) Ponrouch, A.; Marchante, E.; Courty, M.; Tarascon, J.-M.; Palacin, M. R. In Search of an Optimized Electrolyte for Na-Ion Batteries. *Energy Environ. Sci.* **2012**, *5*, 8572-8538.
- (24) Lee, Y.; Lee, J.; Kim, H.; Kang, K.; Choi, N.-S. Highly Stable Linear Carbonate-Containing Electrolytes with Fluoroethylene Carbonate for High-Performance Cathodes in Sodium-Ion Batteries. *J. Power Sources* **2016**, *320*, 49-58.
- (25) Seh, Z. W.; Sun, J.; Sun, Y.; Cui, Y. A Highly Reversible Room-Temperature Sodium Metal Anode. *ACS Cent. Sci.* **2015**, *1*, 449-455
- (26) Komaba, S.; Ishikawa, T.; Yabuuchi, N.; Murata, W.; Ito, A.; Ohsawa, Y. Fluorinated Ethylene Carbonate as Electrolyte Additive for Rechargeable Na Batteries. *ACS Appl. Mater. Interfaces*, **2011**, *3*, 4165-4168.
- (27) Komaba, S.; Murata, W.; Ishikawa, T.; Yabuuchi, N.; Ozeki, T.; Nakayama, T.; Ogata, A.; Gotoh, K.; Fujiwara, K. Electrochemical Na Insertion and Solid Electrolyte Interphase for Hard-Carbon Electrodes and Application to Na-Ion Batteries. *Adv. Funct. Mater.* **2011**, *21*, 3859-3867
- (28) Qian, J.; Henderson, W. A.; Xu, W.; Bhattacharya, P.; Engelhard, M.; Borodin, O.; Zhang, J.-G. High Rate and Stable Cycling of Lithium Metal Anode. *Nat. Commun.* **2015**, *6*, 6362-6370.
- (29) Wang, J.; Yamada, Y.; Sodeyama, K.; Chiang, C. H.; Tateyama, Y.; Yamada, A. Superconcentrated Electrolytes for a High-Voltage Lithium-Ion Battery. *Nat. Commun.* **2016**, *7*, 12032-12040.

- (30) McKinnon, W. R.; Dahn, J. R. How to Reduce the Cointercalation of Propylene Carbonate in Li_xZrS_2 and Other Layered Compounds. *J. Electrochem. Soc.* **1985**, *132*, 364-366.
- (31) Jeong, S.-K.; Inaba, M.; Iriyama, Y.; Abe, T.; Ogumi, Z. Interfacial Reactions between Graphite Electrodes and Propylene Carbonate-Based Solutions: Electrolyte-concentration dependence of electrochemical lithium intercalation reaction *J. Power Sources* **2008**, *175*, 540-546.
- (32) Jeong, S.-K.; Seo, H.-Y.; Kim, D.-H.; Han, H.-K.; Kim, J.-G.; Lee, Y. B.; Iriyama, Y.; Abe, T.; Ogumi, Z. Suppression of dendritic lithium formation by using concentrated electrolyte solutions. *Electrochem. Commun.* **2008**, *10*, 635-638.
- (33) Yamada, Y.; Yaegashi, M.; Abe, T.; Yamada, A. A Superconcentrated Ether Electrolyte for Fast-Charging Li-Ion Batteries. *Chem. Commun.* **2013**, *49*, 11194-11196.
- (34) Yamada, Y.; Furukawa, K.; Sodeyama, K.; Kikuchi, K.; Yaegashi, M.; Tateyama, Y.; Yamada, A. Unusual Stability of Acetonitrile-Based Superconcentrated Electrolytes for Fast-Charging Lithium-Ion Batteries. *J. Am. Chem. Soc.* **2014**, *136*, 5039-5046.
- (35) McOwen, D. W.; Seo, D. M.; Borodin, O.; Vatamanu, J.; Boyle, P. D.; Henderson, W. A. Concentrated Electrolytes: Decrypting Electrolyte Properties and Reassessing Al Corrosion Mechanisms *Energy Environ. Sci.* **2014**, *7*, 416-426.
- (36) Suo, L.; Hu, Y.-S.; Li, H.; Armand, M.; Chen, L. A new class of Solvent-in-Salt Electrolyte for High-Energy Rechargeable Metallic Lithium Batteries. *Nat. Commun.* **2013**, *4*, 1481-1489.
- (37) Yamada, Y.; Chiang, C. H.; Sodeyama, K.; Wang, J.; Tateyama, Y.; Yamada, A. Corrosion Prevention Mechanism of Aluminum Metal in Superconcentrated Electrolytes. *ChemElectroChem* **2015**, *2*, 1687-1694.
- (38) Yamada, Y.; Yamada, A. Review—Superconcentrated Electrolytes for Lithium Batteries. *J. Electrochem. Soc.* **2015**, *162*, A2406-A2423.
- (39) Suo, L.; Borodin, O.; Gao, T.; Olguin, M.; Ho, J.; Fan, X.; Luo, C.; Wang, C.; Xu, K. “Water-in-salt” electrolyte enables high-voltage aqueous lithium-ion chemistries. *Science* **2015**, *350*, 938-943.

- (40) Suo, L.; Borodin, O.; Sun, W.; Fan, X.; Yang, C.; Wang, F.; Gao, T.; Ma, Z.; Schroeder, M.; von Cresce, A.; Russell, S. M.; Armand, M.; Angell, A.; Xu, Kang.; Wang, C. Advanced High-Voltage Aqueous Lithium-Ion Battery Enabled by Water-in-Bisalt⁺ Electrolyte. *Angew. Chem., Int. Ed.* **2016**, *55*, 7136-7141.
- (41) Cao, R.; Mishra, K.; Li, X.; Qian, J.; Engelhard, M. H.; Bowden, M. E.; Han, K. S.; Mueller, K. T.; Henderson, W. A.; Zhang, J.-G. Enabling Room Temperature Sodium Metal Batteries. *Nano Energy* **2016**, DOI: 10.1016/j.nanoen.2016.09.013.
- (42) Schafzahl, L.; Hanzu, I.; Wilkening, M.; Freunberger, S. A. An Electrolyte for Reversible Cycling of Sodium Metal and Intercalation Compounds. *ChemSusChem* **2016**, *9*, 1-9.
- (43) He, M.; Lau, K. C.; Ren, X.; Xiao, N.; McCulloch, W. D.; Curtiss, L. A.; Wu, Y. Concentrated Electrolyte for the Sodium–Oxygen Battery: Solvation Structure and Improved Cycle Life. *Angew. Chem., Int. Ed.* **2016**, *55*, 15310-15314.
- (44) Singh, G.; Acebedo, B.; Cabanas, M. C.; Shanmukaraj, D.; Armand, M.; Rojo, T. An Approach to Overcome First Cycle Irreversible Capacity in P2-Na_{2/3}[Fe_{1/2}Mn_{1/2}]O₂. *Electrochem. Commun.* **2013**, *37*, 61-63
- (45) Yabuuchi, N.; Kajiyama, M.; Iwatate, J.; Nishikawa, H.; Hitomi, S.; Okuyama, R.; Usui, R.; Yamada, Y.; Komaba, S. P2-type Na_x[Fe_{1/2}Mn_{1/2}]O₂ Made from Earth-Abundant Elements for Rechargeable Na Batteries. *Nat. Mater.* **2012**, *11*, 512-517.
- (46) Han, H.-B.; Zhou, S.-S.; Zhang, D.-J.; Feng, S.-W.; Li, L.-F.; Liu, K.; Feng, W.-F.; Nie, J.; Li, H.; Huang, X.-J.; Armand, M.; Zhou, Z.-B. Lithium Bis(fluorosulfonyl)imide (LiFSI) as Conducting Salt for Nonaqueous Liquid Electrolytes for Lithium-Ion Batteries: Physicochemical and electrochemical properties. *J. Power Sources* **2011**, *196*, 3623-3632.
- (47) Cation-Ether Complexes in the Gas Phase: Bond Dissociation Energies of Na⁺(dimethyl ether)_x, x = 1-4; Na⁺(1,2-dimethoxyethane)_x, x=1 and 2; and Na⁺(12-crown-4). *J. Phys. Chem. A* **1997**, *101*, 831-839.

- (48) Yeh, T.-S.; Su, T.-M. Conformational Analysis of Molecular Complexes between Sodium and 1,2-Dimethoxyethane: Photoionization and ab Initio Molecular Orbital Studies. *J. Phys. Chem. A* **1997**, *101*, 1672-1679.
- (49) Evans, T.; Olson, J.; Bhat, V.; Lee, S.-H. Corrosion of Stainless Steel Battery Components by Bis(fluorosulfonyl) imide Based Ionic Liquid Electrolytes. *J. Power Sources* **2014**, *269*, 616-620.
- (50) Yoshida, K.; Nakamura, M.; Kazue, Y.; Tachikawa, N.; Tsuzuki, S.; Seki, S.; Dokko, K.; Watanabe, M. Oxidative-Stability Enhancement and Charge Transport Mechanism in Glyme-Lithium Salt Equimolar Complexes. *J. Am. Chem. Soc.* **2011**, *133*, 13121-13129.
- (51) Lee, J.; Lee, Y.; Lee, J.; Lee, S.-M.; Choi, J.-H.; Kim, H.; Kwon, M.-S.; Kang, K.; Lee, K. T.; Choi, N.-S. Ultraconcentrated Sodium Bis(fluorosulfonyl)imide-Based Electrolytes for High-Performance Sodium Metal Batteries. *ACS Appl. Mater. Interfaces*, **2017**, *9*, 3723-3732.